AD-A179 999 MODIFICATION OF ELECTRON CYCLOTRON MASER OPERATION BY APPLICATION OF AN EXTERNAL SIGNAL(U) NAVAL RESEARCH LAB WASHINGTON DC A H MCCURDY ET AL 31 MAR 87 NRL-9038 1/1

UNCLASSIFIED F/G 9/3 NL

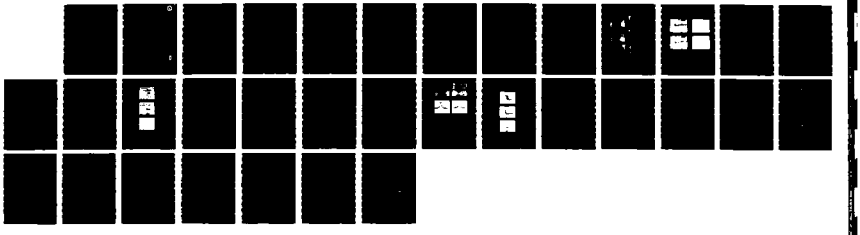

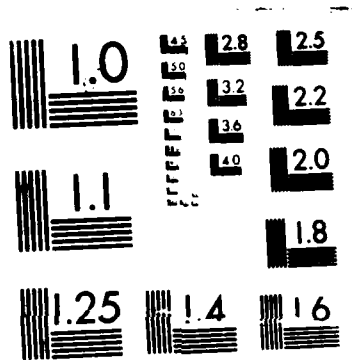

Naval Research Laboratory

Washington, DC 20375-5000

NRL Report 9038

Modification of Electron Cyclotron Maser Operation by Application of an External Signal

A.H. McCURDY AND C.M. ARMSTRONG

Microwave and Millimeter Wave Tube Technology Branch
Electronics Technology Division

W.M. BOLLEN

Mission Research Corporation
Alexandria, Virginia 22312

March 31, 1987

SECURITY CLASSIFICATION OF THIS PAGE

REPORT DOCUMENTATION PAGE

1a. REPORT SECURITY CLASSIFICATION UNCLASSIFIED	1b. RESTRICTIVE MARKINGS
2a. SECURITY CLASSIFICATION AUTHORITY	3. DISTRIBUTION/AVAILABILITY OF REPORT Approved for public release; distribution unlimited.
2b. DECLASSIFICATION/DOWNGRADING SCHEDULE	
4. PERFORMING ORGANIZATION REPORT NUMBER(S) NRL Report 9038	5. MONITORING ORGANIZATION REPORT NUMBER(S)
6a. NAME OF PERFORMING ORGANIZATION Naval Research Laboratory 6b. OFFICE SYMBOL (*If applicable*) Code 6840	7a. NAME OF MONITORING ORGANIZATION
6c. ADDRESS (*City, State, and ZIP Code*) Washington, DC 20375-5000	7b. ADDRESS (*City, State, and ZIP Code*)
8a. NAME OF FUNDING/SPONSORING ORGANIZATION Office of Naval Research/ Office of Naval Technology 8b. OFFICE SYMBOL (*If applicable*)	9. PROCUREMENT INSTRUMENT IDENTIFICATION NUMBER
8c. ADDRESS (*City, State, and ZIP Code*) Arlington, VA 22217	10. SOURCE OF FUNDING NUMBERS PROGRAM ELEMENT NO. 6276N; PROJECT NO.; TASK NO XF62-584-100; WORK UNIT ACCESSION NO. DN480-973

11. TITLE (*Include Security Classification*)

Modification of Electron Cyclotron Maser Operation by Application of an External Signal

12. PERSONAL AUTHOR(S)

McCurdy,* A.H., Armstrong, C.M., and Bollen,† W.M.

13a. TYPE OF REPORT	13b. TIME COVERED	14. DATE OF REPORT (*Year, Month, Day*)	15. PAGE COUNT
Final	FROM _____ TO _____	1987 March 31	33

16. SUPPLEMENTARY NOTATION

*Also at Section of Applied Physics, Yale University, New Haven, Connecticut 06520

†Mission Research Corporation, Alexandria, Virginia 22312

17. COSATI CODES		
FIELD	GROUP	SUB-GROUP

18. SUBJECT TERMS (*Continue on reverse if necessary and identify by block number*)

Gyroklystron, Gyrotron, Primed oscillator, Phased-locked oscillator

19. ABSTRACT (*Continue on reverse if necessary and identify by block number*)

Operation of the electron cyclotron resonance maser (ECRM) when subjected to an external rf signal is studied. The signal is introduced both by direct injection through a coupling hole in the oscillator and by modulating the electron beam in separate cavities, upstream of the oscillator. Experiments using both one and two "pre-bunching" cavities are reported. It is found that the gyromonotron, a specific embodiment of the ECRM, can be phase locked by premodulating the electron beam. In this case, the required drive power levels are more than 15 dB below that predicated by Adler's widely applicable theory for single-cavity oscillators. In addition, the same method allows oscillator priming at drive powers 50 dB below that required by magnetrons for equivalent phase control. As with other phase-locked systems, significant reduction of frequency and amplitude noise is observed within the locking band. In the pulsed oscillator, reduction of starting time jitter by almost an order of magnitude occurs, even with a priming signal of a power level 65 dB below that of the oscillator. The general amplitude and frequency response of the ECRM to an applied external signal is also investigated. Three distinct regions of qualitatively different behavior are noted: soft excitation, which is free, self-excited oscillation; hard excitation, where the oscillation requires an external impulse for start-up; and amplifier, in which the output power level and frequency are linearly related to the drive in the small signal regime.

20. DISTRIBUTION/AVAILABILITY OF ABSTRACT	21. ABSTRACT SECURITY CLASSIFICATION
☒ UNCLASSIFIED/UNLIMITED ☐ SAME AS RPT ☐ DTIC USERS	UNCLASSIFIED
22a. NAME OF RESPONSIBLE INDIVIDUAL Alan H. McCurdy	22b. TELEPHONE (*Include Area Code*) (202) 767-3936 22c. OFFICE SYMBOL Code 6842

DD FORM 1473, 84 MAR 83 APR edition may be used until exhausted
All other editions are obsolete

SECURITY CLASSIFICATION OF THIS PAGE

☆U.S. Government Printing Office: 1985—607-047

CONTENTS

MODIFICATION OF ELECTRON CYCLOTRON MASER OPERATION BY APPLICATION OF AN EXTERNAL SIGNAL

INTRODUCTION

Since the early 1960s when the electron cyclotron resonance maser mechanism was first understood and demonstrated [1-3], research has progressed toward using this mechanism to produce coherent microwave and millimeter-wave radiation at unprecedented power levels. The maser interaction consists of one branch of the fast, right-hand circularly polarized, cyclotron beam wave coupling to a superluminous electromagnetic wave. One practical embodiment of this interaction using a MIG gun with a cavity oscillator is called the gyromonotron [4]. Because no intricate slow wave structure is required to couple the electromagnetic wave to the beam wave, the gyromonotron avoids electrical breakdown problems and alleviates thermal wall loading at high frequencies and powers. The performance of the gyromonotron has been impressive, with microsecond pulse powers over 600 kW at frequencies well over 100 GHz [5,6], and continuous-wave (CW) powers of 100 kW at 140 GHz [7]. Two of the remaining problems are mode stabilization in the cavity oscillator (because the cavity dimensions must be large compared to a wavelength at high powers and frequencies) and higher efficiency operation. It may be possible to address both of these problems by properly coupling a drive signal onto the electron beam to provide current density modulation before the beam reaches the gyromonotron [8,9]. The mode control feature is similar in spirit to that of the complex cavity gyromonotron [10] that was shown in an experiment to be capable of an electronic efficiency of $> 60\%$ [11]. Our system, however, uses a separate cavity below the start oscillation threshold and an external signal to provide the modulation, as in the gyroklystron amplifier [12,13]. There have been predictions that the highest efficiency regime of operation for the gyromonotron is below the start oscillation current in the *hard-excitation* regime [14]. The characteristic of this regime is that the gyromonotron requires an initial cavity field amplitude, well above the noise level, to oscillate. One of the proposed means of accessing this regime is to adjust the magnetic field once the oscillation has started. Our experiment shows that it is possible to operate in the hard excitation regime by applying an external signal.

As has been done on other microwave oscillators [15,16], we investigate methods of obtaining phase control over the output of the gyromonotron. The motivation for this work is that while phase control is required in a number of important applications, oscillators generally have larger electronic efficiencies and are somewhat more compact than amplifiers. The two methods investigated here are phase locking and priming by application of an external signal. In this work, a novel means is used to couple the drive signal into the oscillator. This is to pre-modulate the electron beam in a separate cavity.

Free running, pulsed oscillators tend to be noisy. There is a fair amount of randomness in the start-up time in the pulsed oscillator since the fields build up from rf noise that is generated by beam current density fluctuations or beam cyclotron motion. Also, because of slight variations in the beam conditions, there is pulse-to-pulse jitter in the oscillation frequency and amplitude. These noise problems can be somewhat alleviated by injection of a stable external signal.

All of the previous topics, with the exception of mode control, are studied by using the Naval Research Laboratory's (NRL's) 4.5 GHz gyroklystron circuit [17,18]. The following sections summarize the experimental setup, results on phase control, noise suppression, and observations of qualitatively different regimes of response to external excitation.

Manuscript approved December 12, 1986.

EXPERIMENTAL SETUP

The NRL three-cavity gyroklystron circuit is shown in Fig. 1. A magnetron injection gun produces a thick annular electron beam which then interacts with the cavity electromagnetic fields. The drift sections between the cavities are cut off to the 4.5 GHz radiation and provide ~30 dB of intercavity isolation. All three cavities are rectangular and operate in the TE_{101} mode at 4.5 GHz. Each cavity is tunable by means of a movable diaphragm in one of the side walls. In normal gyroklystron amplifier operation, the beam conditions are such that all three cavities are below the start oscillation threshold. It is possible to excite an oscillation in any of the cavities, however, by appropriately profiling the magnetic field along the axis of the device and increasing the perpendicular-to-parallel velocity ratio α of the beam. As can be seen in Fig. 1, waveguide couples out radiation from each of the cavities so that the fields in each cavity can be monitored. The first two cavities are identical in construction (.9 λ in length, $Q_L \approx 650$, $Q_e \approx 1100$, undercoupled), while the third cavity is somewhat longer (1.1 λ and $Q_L \approx 300$, $Q_e \approx 375$, overcoupled). Here, Q_L and Q_e are the loaded (cold cavity) and external quality factors, respectively.

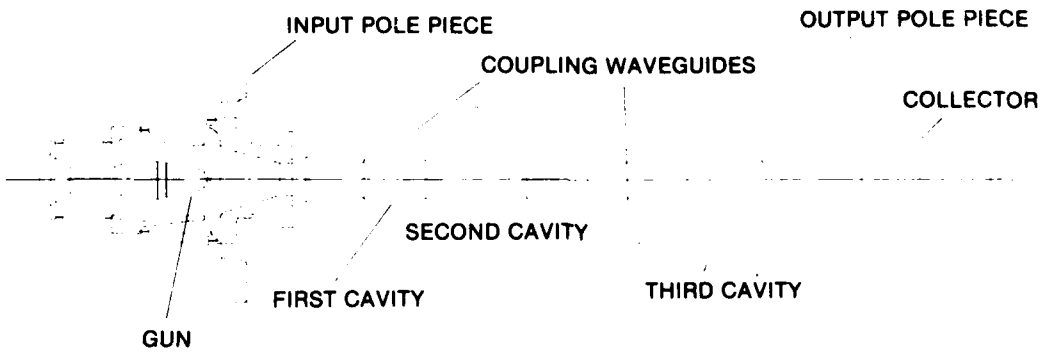

Fig. 1 — Three-cavity gyroklystron circuit

Since the cavity fields interact with the beam at the fundamental, relativistic electron cyclotron frequency, an axial magnetostatic field of 1.6 kG is required. The experiment uses an electron beam with a 60 Hz repetition rate of 4.0 μs pulses. The beam voltage is near 30 kV, and the beam currents are 5 to 6 A. The beam α is in the range 1.0 to 1.2 for two- and three-cavity operation but is somewhat higher when an oscillation is excited in cavity 1 (~ 1.3 to 1.5). These values for α are determined from measurements of radiation frequency and beam energy, together with the uncoupled dispersion diagrams of the cavity/beam system as well as from theoretically predicted gyroklystron gain in the multicavity situation.

GYROMONOTRON PHASE LOCKING

Phase locking by direct injection of an external signal has been a common method of achieving phase control over oscillators. The first experiments were done on electron tube circuits [19-21] and later on microwave oscillators [16,17] and lasers [22,23]. The phase-locking phenomenon can be understood from the following discussion. The self-excited free oscillator is described by the following equation in the lumped circuit approximation:

$$d^2V/dt^2 - (\eta - \beta V^2)dV/dt + \omega_0^2 V = 0. \quad (1)$$

Here, V is the voltage across the cavity "terminals," and η and β are small positive constants that represent the phenomena of linear growth and saturation in the oscillator. The nonlinear term is necessary for the self-excited oscillator to achieve a steady state. In the steady state, the saturation and growth terms exactly cancel (thus the steady-state voltage amplitude V_s is $\sqrt{\eta/\beta}$), and the oscillation proceeds at frequency ω_0 plus higher harmonics. If a driving term of the form $\omega_d^2 V_d \cos(\omega_d t)$

(V_d is proportional to the amplitude of the drive signal) is added to the right-hand side of Eq. (1), the new solutions for $V(t)$ fall into two classes. This can be seen by applying the method of slowly varying amplitude and phase to Eq. (1). It is assumed that the oscillation and drive phase angles vary rapidly at the oscillation frequency ω_0 and that the oscillation amplitude and phase with respect to the drive signal vary slowly on a time scale of $\omega_0 - \omega_d$. Using this method, two coupled equations can be obtained; one describes the amplitude evolution in time, and the other,

$$d\Phi/dt = \omega_o - \omega_d + (\omega_d/2)V_d/V \sin\Phi, \tag{2}$$

describes the evolution of the relative phase angle Φ between the external signal and the oscillator. Equation (2) is referred to here as Adler's equation. For small applied signals ($V_d << V_s$), the amplitude and phase equations can be decoupled by using the steady-state amplitude for V in Eq. (2). The time-independent solution for Φ, the phase locked condition, is immediately obtained by setting $d\Phi/dt = 0$:

$$2(\omega_d - \omega_0)/\omega_d V_s/V_d = \sin\Phi. \tag{3}$$

Since $\sin\Phi$ is always ≤ 1, it is clear that locking can only take place for

$$2|\omega_d - \omega_0|/\omega_d V_s/V_d \leq 1. \tag{4}$$

This relation gives the allowable drive frequency band that will maintain locking of a given oscillator at a given external signal amplitude. If this condition for locking is not met, then $d\Phi/dt \neq 0$, and there is a continual phase slippage between the drive signal and oscillation. This slippage will manifest itself in a nonsinusoidal beat signal at a frequency of $\sim \omega_d - \omega_0$. In summary, the nonlinear oscillator described by Eq. (1) with a sinusoidal forcing term can oscillate at the drive frequency if the condition of Eq. (4) is met. If this condition is satisfied, the oscillator is in the phase-locked state.

Slater [24] has developed a more convenient form of Eq. (4) for microwave oscillators operating into a matched load:

$$Q_e|\omega_d - \omega_0|/\omega_0\sqrt{(P_0/P_d)} \leq 1, \tag{5}$$

where the subscripts d and o refer to the drive signal and oscillator as before, and P is power. As stated, Q_e is the external Q of the oscillator cavity. The ω_0 in the denominator of Eq. (5) can be replaced by ω_d as in Eq. (4), since the correction is one of higher order.

An alternative means of coupling the drive signal into the oscillator is by means of current density modulation in the electron beam. This modulation can be done by passing the beam through a separate cavity to which the drive signal is applied. The theoretical analysis of this method [9,14] has predicted that a smaller drive power would be required to phase lock the free oscillation at a given frequency difference ($\omega_d - \omega_0$) for electron beam pre-modulation than for the direct-injection case. We experimentally compare these two methods of phase locking the gyromonotron.

Phase-Locking Diagnostics

Several diagnostics are used to determine the onset of the phase-locked state. Figure 2 is a schematic of the experimental setup. The input and output frequencies are monitored by digital frequency meters (a pulse counter measures the output frequency). As the gyromonotron becomes locked, the output frequency shifts to the value of the drive frequency. The fact that the drive frequency remains unchanged throughout the locking process is evidence that the driver is not being locked by the gyromonotron. A spectrum analyzer is used to monitor the frequency content of the gyromonotron output. When the drive signal is sufficiently close in frequency to the oscillation, a peak corresponding to this frequency appears in the output spectrum. As the drive power is increased, the gyromonotron peak merges with the peak at the drive frequency. The drive and output

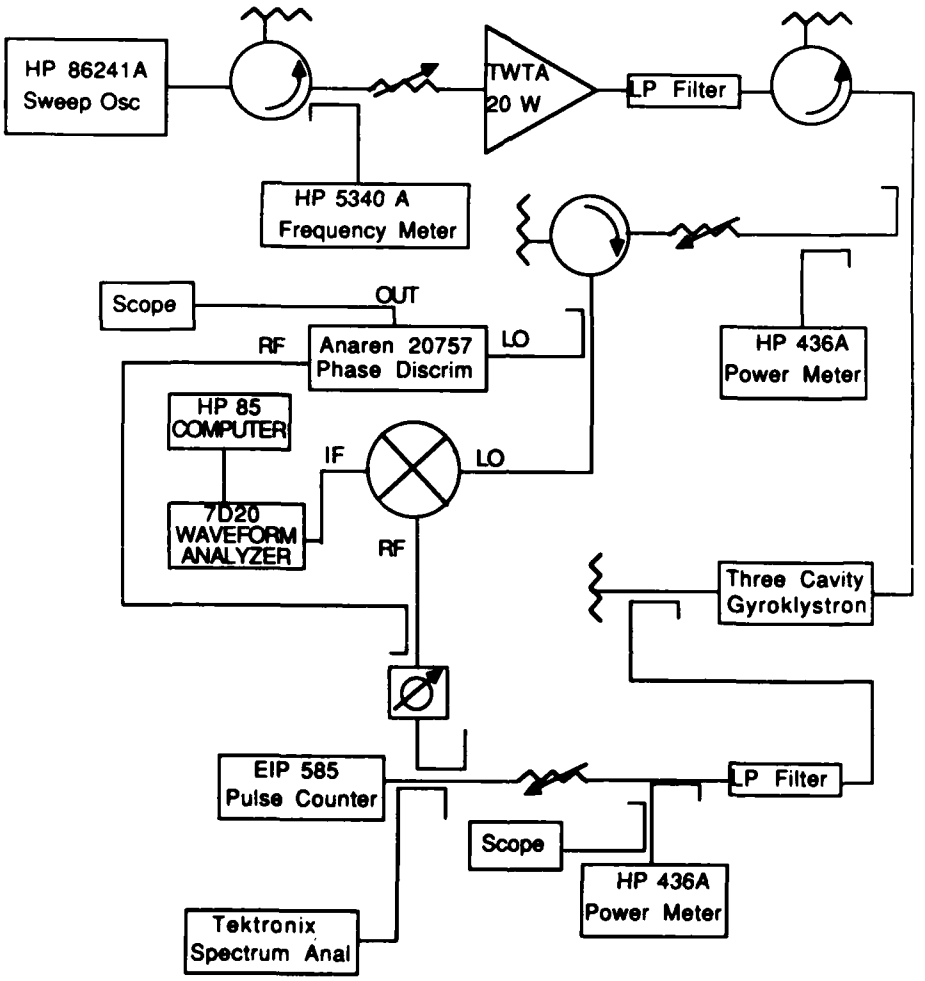

Fig. 2 — Experimental setup

signals are then mixed, and the IF output displayed on an oscilloscope. The beat signal, which is present in the unlocked state, discontinuously vanishes as the transition to the locked state takes place. This same phenomenon can be observed directly on a crystal diode as amplitude modulation in the gyromonotron output owing to the presence of the two frequencies. Finally, a phase discriminator [25] provides a polar display of the change with time of the relative phase between the driver and oscillator. Figure 3 shows the output of each of these diagnostics as the oscillator passes from the free to the locked state. Shifting the phase of the driver and making sure that the oscillator phase follows verifies that the gyromonotron is locked to a constant phase angle with respect to the drive. The steady-state locking angle is found to vary between $\pm 90°$ as would be expected from Eqs. (3) and (4).

Direct-Injection Phase Locking

It has been shown previously that a gyromonotron can be phase locked by the direct injection method [26]. We verify those results by phase locking an oscillation in cavity 1. The plotted points in Fig. 4 show the drive power required to lock the cavity 1 oscillation at a given frequency separation between oscillator and driver. The gyromonotron is phase locked in the entire region between the two sets of points. The solid curves in the same figure show the phase-locking limits predicted from the time-independent solution (Eq. 4) of Adler's equation. The agreement between the experimental results and theory is quite good for small drive power (the theory assumed $V_d << V_s$). The oscillation strength in cavity 1 is ~ 1 kW. Care is taken to assure good isolation between the driver system and the output radiation from cavity 1. Direct injection-locking, as a technique, is hampered by the fact that the drive radiation must be launched through the output line of the oscillator by means of a circulator. There is always the danger of locking or damaging the driver if adequate isolation from the oscillator is not present.

Phase-Locking by Pre-Modulation of the Electron Beam

Cavity 2 is phase locked by applying the drive signal to cavity 1. The 30 dB isolation between the cavities prevents the input signal from leaking directly into the cavity 2 oscillator. Although cavities 1 and 2 are identical in construction, it is possible to keep cavity 1 quiescent by tuning the doppler-shifted electron cyclotron frequency well above the cavity resonant frequency. This is done by raising the magnetic field in cavity 1 and mechanically lowering the cold cavity resonant frequency. Unfortunately, in this condition cavity 1 is not able to absorb radiation very well at the frequency at which cavity 2 is oscillating. The results of this two-cavity locking system are shown in Fig. 5. Here, once again, the locking bandwidth is shown for different drive-to-oscillator power ratios. The experimental locking width is considerably wider than the Adler prediction, again shown by the solid curves. This difference is because of an intensification of electron beam modulation between the input and output cavities due to the same gain mechanism that operates in the gyroklystron amplifier (regenerative amplification in cavity 1 and gain due to ballistic phase bunching of electrons in the drift section). Thus, by using a prebunching cavity, problems of driver protection are circumvented and the drive signal can be enhanced in transit to the gyromonotron.

Figure 6 shows the further increase in locking bandwidth that is obtained by using two cavities to pre-modulate the beam. Cavity 3 is run as a free oscillator, and the drive signal is injected into cavity 1. Note that the locking width predicted by Adler in Fig. 6 is much larger than in Fig. 5 at a given power ratio because Q_e for cavity 3 is only 375. The three-cavity system allows locking at more than 15 dB below the Adler limit. The two-cavity gain in the amplifier mode is 10 to 20 dB; this accounts for the 15 dB improvement. In this experiment we find that the cavity resonant frequencies should be stagger tuned for most efficient phase-locked operation. This is due to the increased frequency pushing effect of the electron beam as the bunching process takes place. The frequency of maximum absorption of cavity 1 is ~ 10 MHz higher than the cold cavity resonance, while the maximum emission from cavity 3 comes at 60 MHz above the cold resonance. To make these frequencies equal, the resonant frequency of the third cavity is mechanically tuned downward by ~ 50 MHz. Cavity 2 is tuned to a cold resonant frequency approximately halfway between the other two.

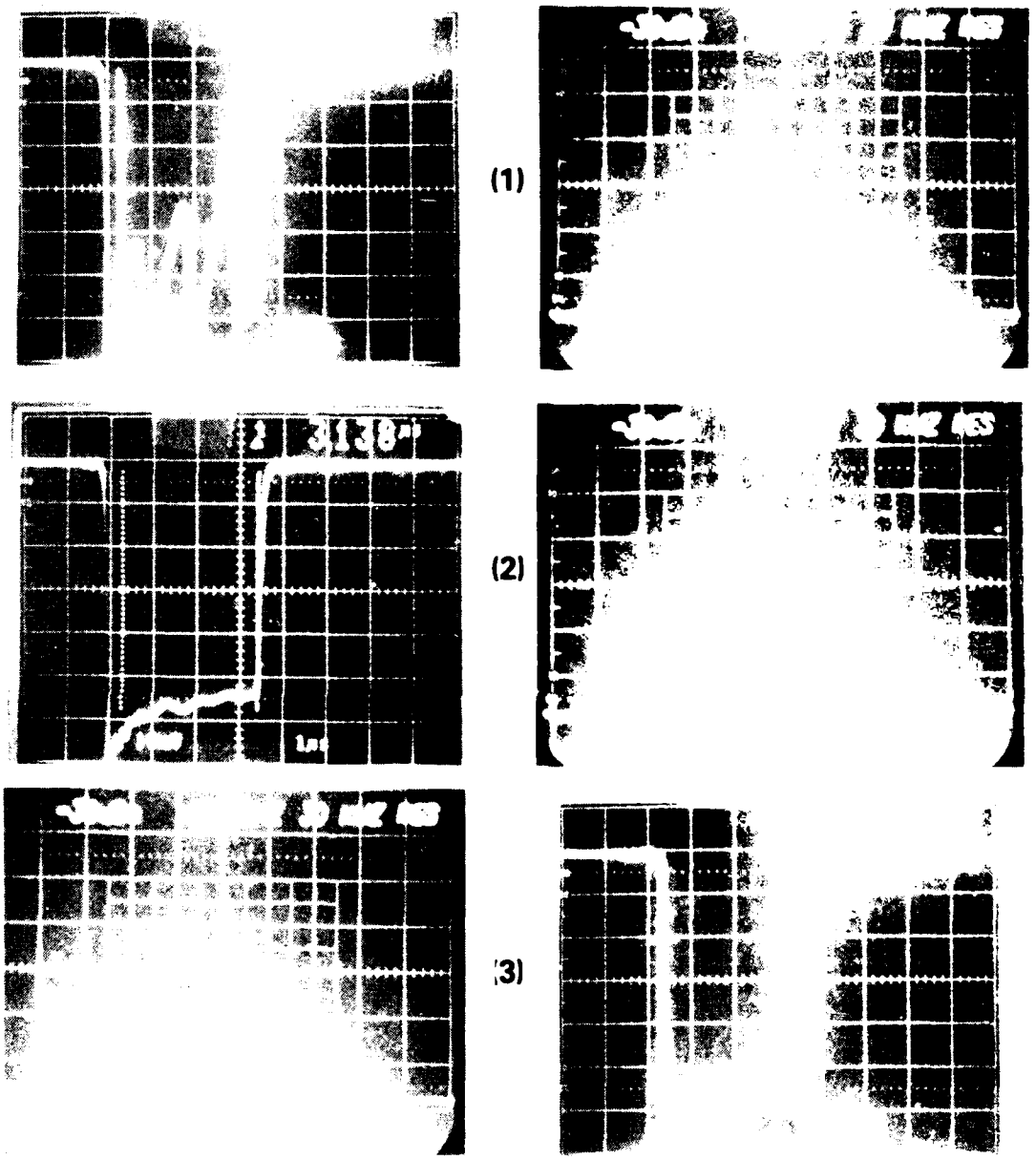

(a) Crystal diode output (b) Spectrum analyzer output

Fig. 3 - Output of diagnostics as gyromonotron is phase locked by increasing the drive power. (1) Locking edge; (2) locked oscillation; and (3) free oscillation.

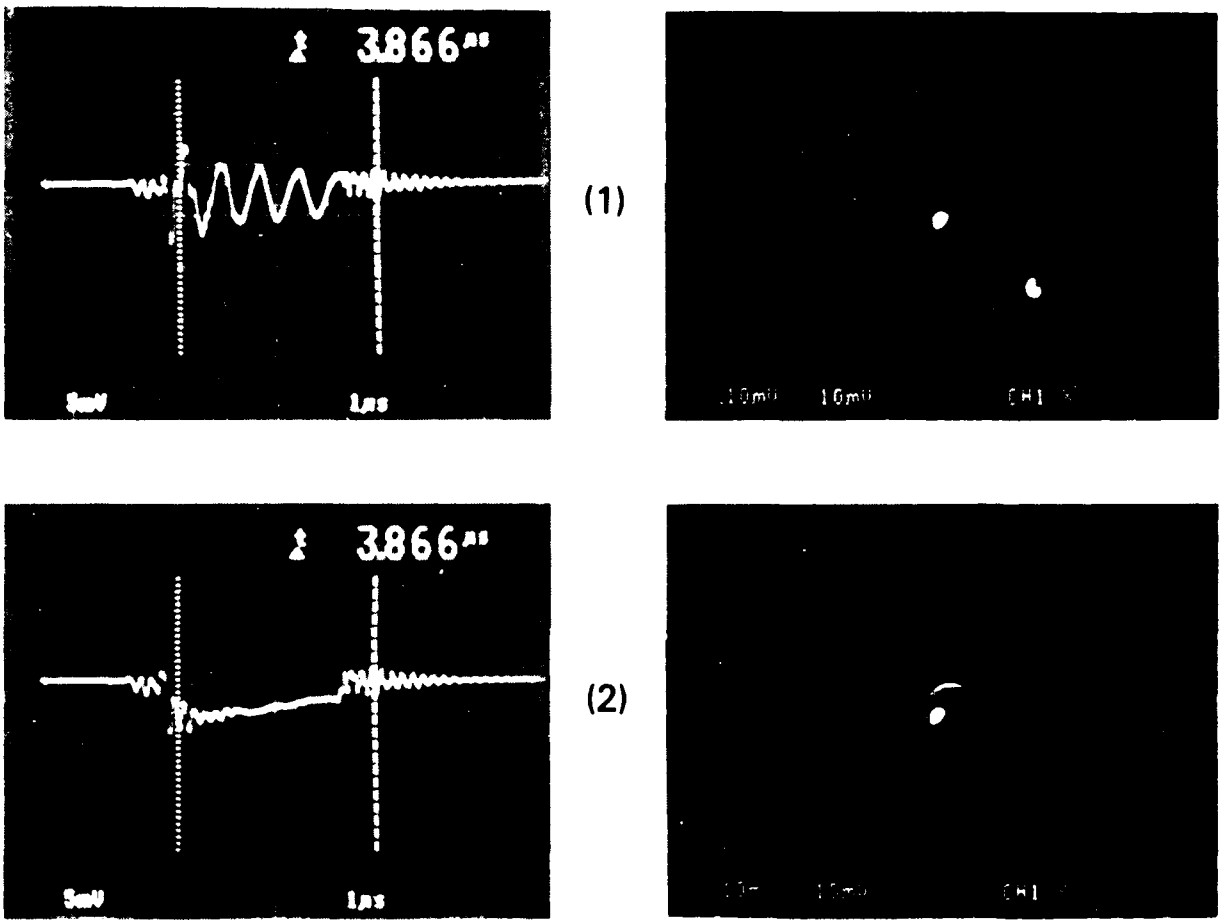

(c) Mixer phase detector output

(d) Phase discriminator output

Fig. 3 (Continued) — Output of diagnostics as gyromonotron is phase locked by increasing the drive power (1) Locking edge, (2) locked oscillation; and (3) free oscillation.

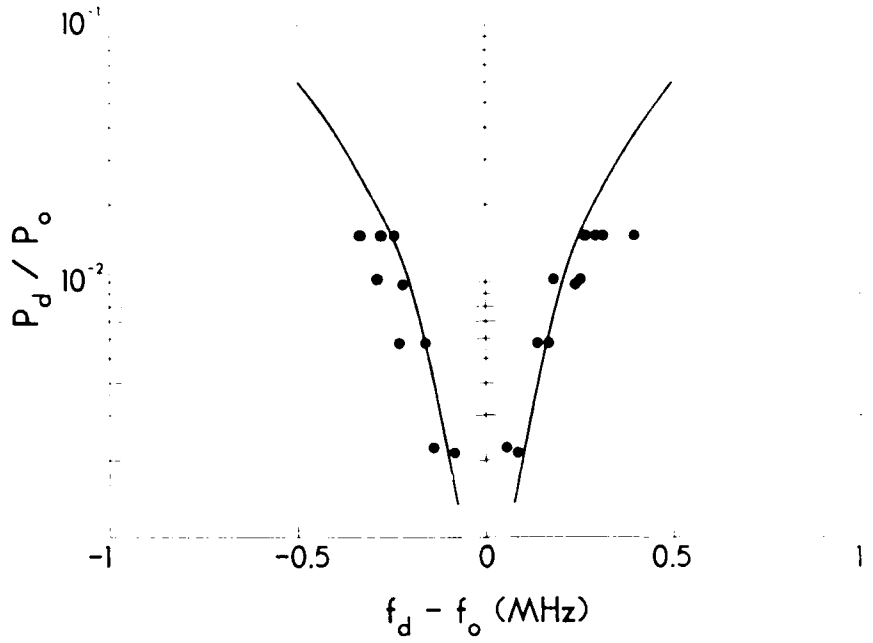

Fig. 4 — Phase locking by direct injection of rf into cavity 1

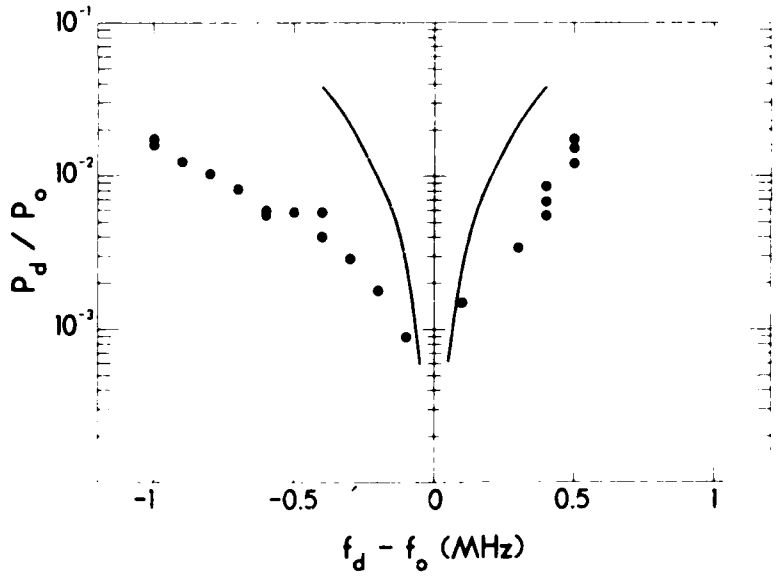

Fig. 5 — Phase locking cavity 2 gyromonotron by pre-modulating the beam in cavity 1

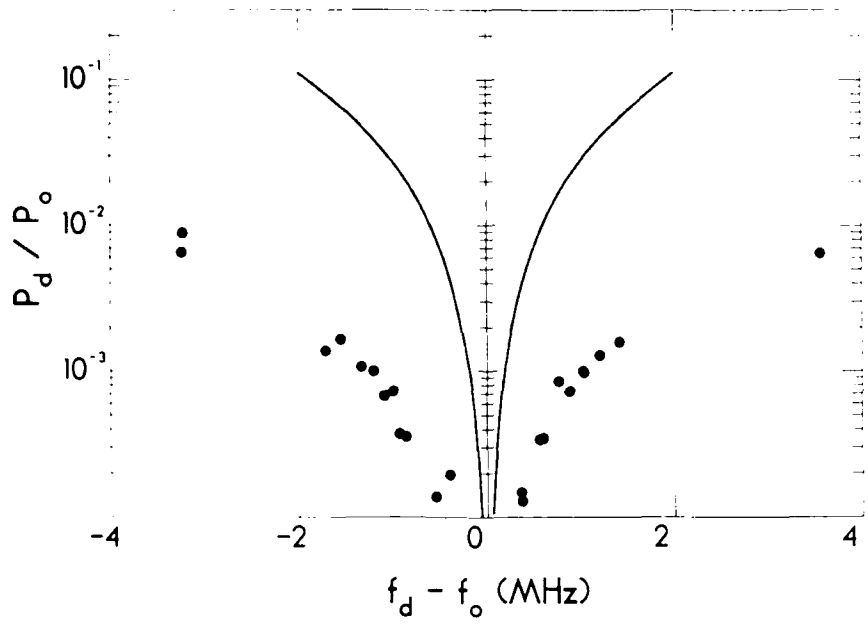

Fig. 6 — Phase locking cavity 3 gyromonotron by using two cavities to pre-modulate the beam

In summary, the results indicate that a gyromonotron is most effectively phase locked by introducing a modulated electron beam into the oscillator. The advantages over direct injection locking include potential gain of the drive signal upon traversal of the drift sections and intermediate cavities and natural separation between the driving components and the cavity oscillator. This separation allows both protection of the driving components and more effective coupling of the drive signal onto the beam.

Another phase-locking issue briefly investigated is that of phase locking by a large drive signal. Figure 7, where data are taken from a two-cavity experiment, shows extreme asymmetry and expanded locking width compared to the Adler prediction. The fact that the locking width exceeds the Adler prediction at large drive powers agrees qualitatively with gyromonotron direct-injection measurements in a previous experiment [26]. It is understandable since Adler's result is based on a small-signal approximation. The asymmetry in locking width is due to two effects. The first is the dependence of the pre-modulation section gain on frequency, and the second is the effect of mode suppression. In the experimental study of the gyroklystron amplifier, the highest gain of the device was measured to occur at a lower frequency than the frequency of greatest absorption in cavity 1. This is true when the magnetic field profile is flat and the cavities are tuned to the same resonant frequency. In our case, cavity 2 oscillates at a higher frequency than the cavity 1 maximum absorption frequency. The frequency of highest gain through the first drift section is then lower than the cavity 2 oscillation frequency. Hence, the lower frequency drive signal appears larger at cavity 2, and there is a corresponding shift in the locking band (this effect is noted to a lesser degree in the small signal cases as well). Note that the total locking width in Fig. 7 is limited to ~8 MHz, which is the bandwidth of cavity 1. The second reason for the asymmetry in locking width is the presence of an entirely different phenomenon on the lower locking edge. The process of unlocking is observed to be different on the upper and lower locking edges. The upper edge exhibits the normal sudden appearance of a large beat signal in the output of the mixer diagnostic as the oscillator unlocks. At the lower locking edge, the beat signal that appeared seemed to grow from zero amplitude as the drive frequency was lowered. The curve shown on the left-hand side of Fig. 7 marks the frequencies at which this small beat signal first became visible. This growth in amplitude of the beat signal indicates that the free oscillation in cavity 2 is being suppressed rather than locked by the drive signal along this lower "locking edge." The area where this suppression might be occurring is indicated by

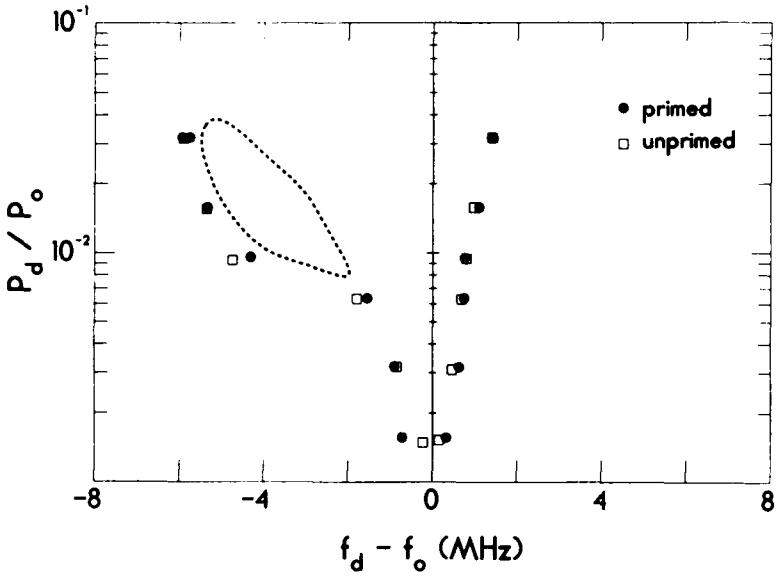

Fig. 7 — Phase locking with large drive signal; drive not present during oscillation buildup (unprimed), overlapped (primed), and estimated region of mode suppression (dash)

the dashed contour in Fig. 7. Within this region, the drive signal initiates an oscillation that competes with the self-excited oscillation in cavity 2. The theory of this type of multimode interaction has been discussed briefly in the gyromonotron literature [27-29] as well as in more detail in that of lasers [23]. In the two-mode gyromonotron, it is usually found that the oscillation that starts first (the driven one in our case), tends to suppress the other.

By pulsing the driver, the locking limits are independent of the turn-on sequence of driver and gyromonotron. The pulse-to-pulse phase coherence, however, is degraded if the drive signal is introduced after the buildup of the oscillation.

GYROMONOTRON PRIMING

Priming, or phase initiation of a pulsed oscillator by a CW driver, was observed experimentally and analyzed theoretically in the early research into controlling the phase of magnetrons [15,30,31]. Recent work has also been done on solid-state oscillators [32-34] and magnetrons [35-37]. The pulsed oscillation, though self-excited, grows from an initial condition of random noise. This results in total phase incoherence between one oscillator pulse and the next. The introduction of a stable, CW external signal during the oscillation buildup increases the amount of interpulse phase coherence. The amount of start-up phase jitter in the presence of this external priming signal can be estimated by using the method of David [30]. A lumped circuit representation of the oscillator is used so the oscillator amplitude and phase can be represented by a single complex voltage. The analysis starts with an estimation of the preoscillation conditions in the gyromonotron. Small variations in electron current density excite fluctuating voltages in the oscillator cavity. Though the noise is wideband, the presence of the cavity filters all but a narrow band of frequencies within a range determined by the cavity Q factor. Thus the noise frequency is reasonably close to that of the injected signal although its phase varies randomly. The noise amplitude varies statistically about some mean. The net voltage in the cavity is given by the vector sum of the injected signal and the noise signal (see Fig. 8). It is clear that the phase of the net voltage will vary over a smaller range as the amplitude ratio between the signal and noise becomes larger. The probability of start-up at a given phase can be determined as a function of the rms signal-to-noise ratio once the statistical behavior of the noise amplitude is known. From the half-width of this probability distribution, a root-mean-square deviation in start-up

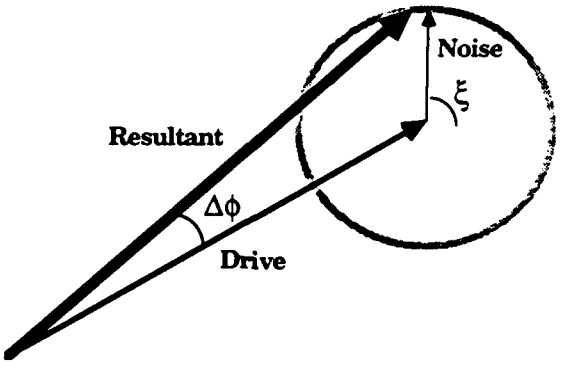

Fig. 8 — Phase diagram of voltage signals during priming of oscillation. The noise voltage varies randomly in phase, but resultant voltage (that from which the oscillation grows) is constrained to a phase of ± ΔΦ about the drive.

phase can be found. This value can be compared directly with experimental results. This comparison, using some measurements of gyromonotron preoscillation noise, will be made in a later work. Here, we simply use the rms phase jitter at the oscillation pulse start-up to determine the degree of control that the drive signal exerts. It should be emphasized that this priming phenomena does not control the frequency of the oscillator. A separate system, such as a phase-locked loop [38], must be used if phase coherence is required throughout the pulse.

The oscilloscope traces in Fig. 9 show the priming effect. These are taken from an experiment where cavity 2 is oscillating, and the external signal is applied to cavity 1. The pictures each show, from top to bottom, the gyromonotron rf output, the gated drive signal pulse, and the phase detector output resulting from mixing the drive and gyromonotron rf signals. The drive chain comprises the CW system shown in Fig. 2 with a mixer, acting as an rf gating switch, inserted before the traveling-wave tube amplifier (TWTA). The mixer can be operated in this manner by applying a trigger pulse to the intermediate-frequency (IF) port and the CW rf to the local oscillator (LO) port. The switch has a fast rise time (< 10 ns, limited by gate pulse rise time) and provides about a 30 dB differential between the on and off positions. Part of the CW drive is diverted to the output diagnostics (shown in Fig. 2) before being gated by the switch. Thus the output of the phase detector (shown at the bottom of the oscillographs in Fig. 9) occurs over the time span of the whole width of the gyromonotron rf pulse instead of only the width of the drive pulse. The drive power is ~ 60 dB down from the oscillator power in this figure. It can be seen from the phase detector traces in Figs. 9(a) and 9(b) that the priming effect does not occur unless the drive signal is present within a window ~ 300 ns wide during the oscillation buildup. The blurred output (scope triggered at 60 Hz, photo exposure time ~ 2 s) of the phase detector verifies that the start-up phase varies almost randomly from pulse-to-pulse in the gyromonotron in these cases. The well-defined phase detector output in Fig. 9(c) reveals that each pulse of the gyromonotron is starting up in phase with the driver. Note that this priming effect is occurring with a drive signal only ~ 100 ns wide. The interpretation is that only during a brief interval is the priming signal large compared to the oscillation and thus able to have an effect.

In all the subsequent priming experiments to be discussed, the drive pulse is much longer in duration than the gyromonotron pulse. This is simply to assure that there is enough overlap on the leading edge. Directional couplers are used to reduce the drive signal into cavity 1 to a low level while allowing the drive oscillator to operate at a high power (10 to 20 W). This reduces the chance of any feedback from the gyromonotron into the driving circuit. Fig. 10 shows the degree of pulse-to-pulse phase control achieved with different levels of priming power when the drive signal is injected directly into the gyromonotron (cavity 1). The rms phase jitter is measured by taking the

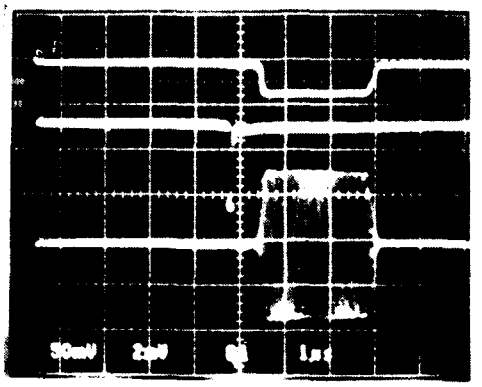

(a)

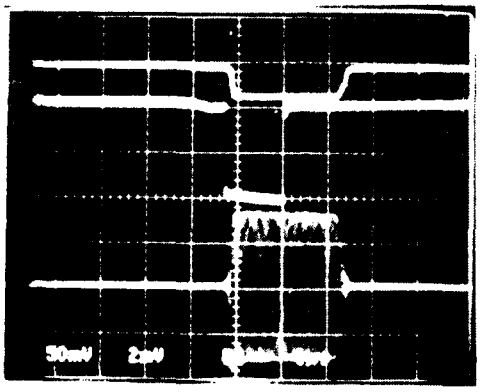

(b)

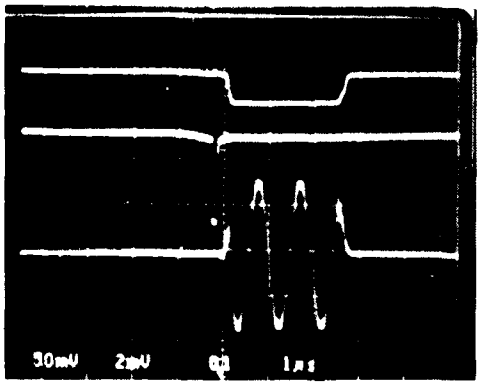

(c)

Fig. 9 — Priming phenomenon. Oscillographs show (from top) gyromonotron rf output, rf drive signal, and the two signals mixed. (a) Drive pulse arriving too early; (b) drive pulse too late (even though widened by a factor of 10; (c) drive at correct time.

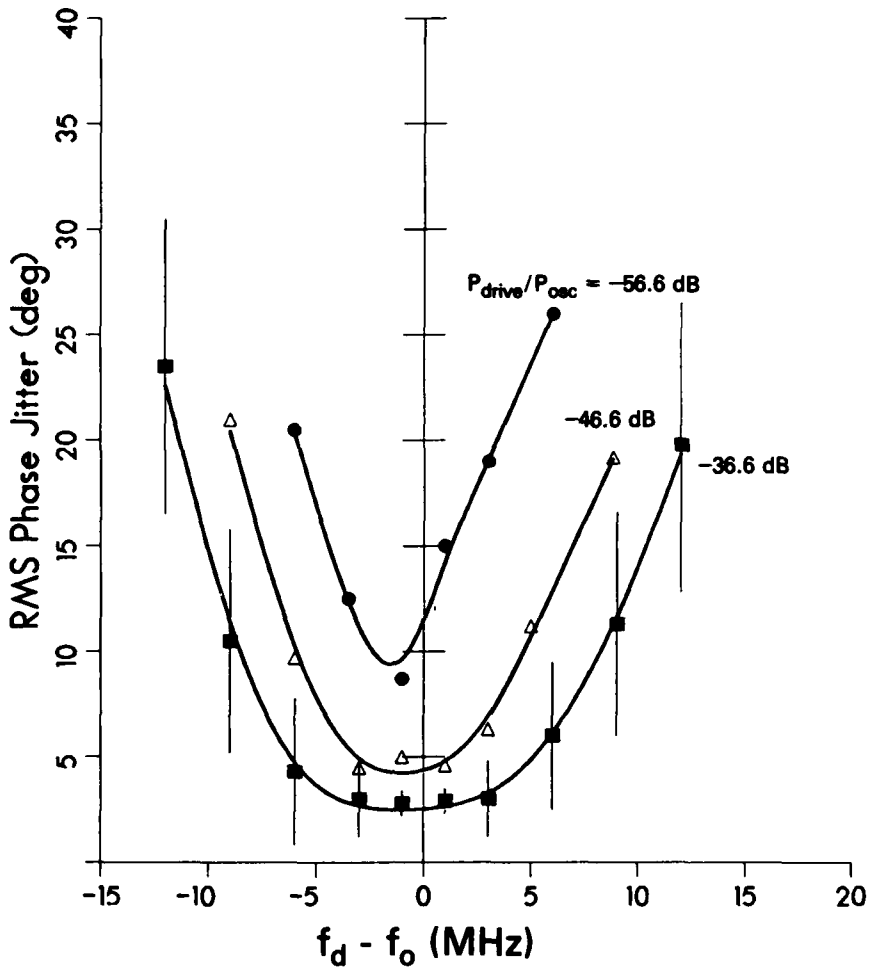

Fig. 10 — Degree of control of initial start-up phase by various levels of direct-injection priming power

standard deviation of the voltage output of the phase detector at a point in time near the start of the oscillation. By using the front of the pulse only, any phase shift due to pulse-to-pulse frequency variation is avoided. Pulse-to-pulse amplitude variation does affect these measurements; however, this source of error is small. The degree of phase control diminishes both as the frequency separation between the driver and oscillator is increased and as the drive power is decreased. Note that the bandwidth over which there is significant phase control is on the order of the cavity 1 bandwidth (8 MHz). This is much larger than the bandwidth over which phase locking takes place when using similar drive power. The error bars shown in the figure increase with frequency offset because the beat signal becomes less well-resolved on the digital oscilloscope at higher frequencies. These errors are the same for all data taken at a given frequency offset.

The priming curves obtained when the drive signal is applied to a pre-bunching cavity are shown in Fig. 11. Because of amplification through the first cavity and drift section, priming can be achieved at much lower drive powers than in the single-cavity case. The degree of phase control is not extremely sensitive to changes in drive power in the range −50 to −70 dB. Therefore, the bandwidth over which better than 5° control is exerted is almost twice that of cavity 1. Figure 12 gives the result of using two pre-bunching cavities. Now, phase control of better than 5° is attained at drive powers 90 dB down from the oscillator power. This performance is far better than any other priming system of which the authors are aware. Magnetrons provide phase control to within 2° at drive powers 20 dB below the oscillator power [39]. Our system controls the phase to the same

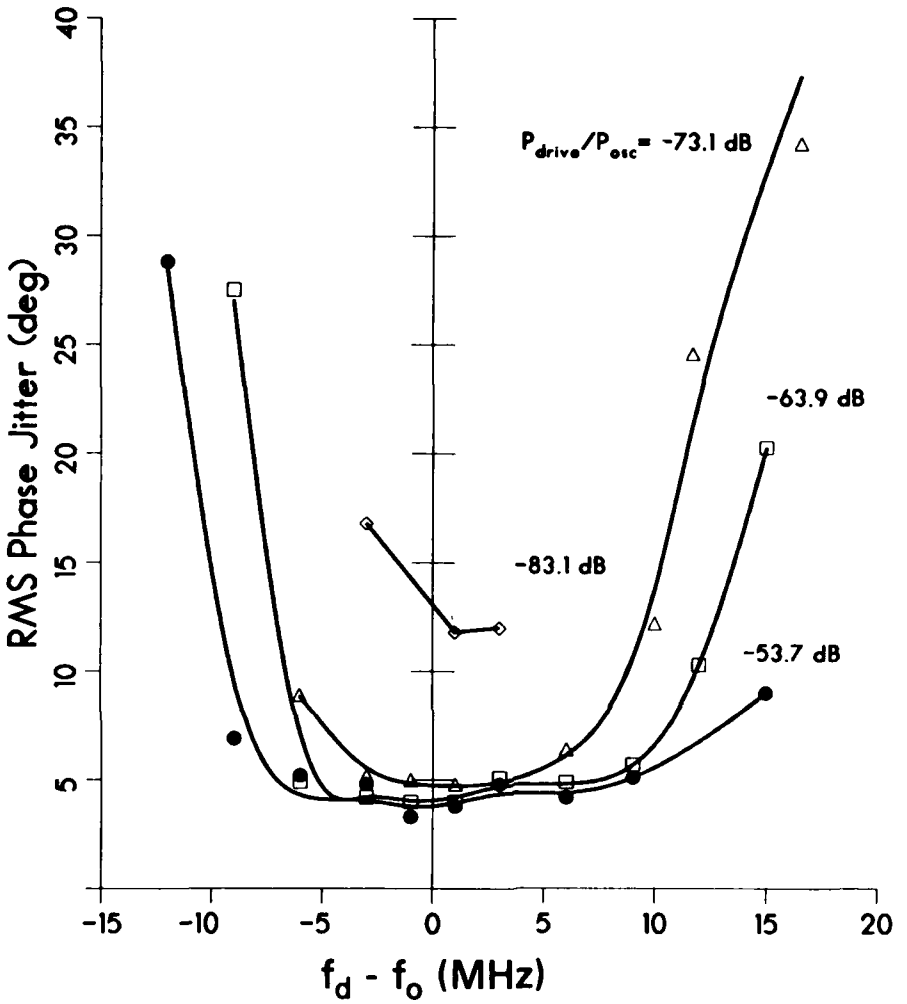

Fig. 11 — Degree of control of start-up phase of cavity 2 oscillation by applying priming signal to cavity 1

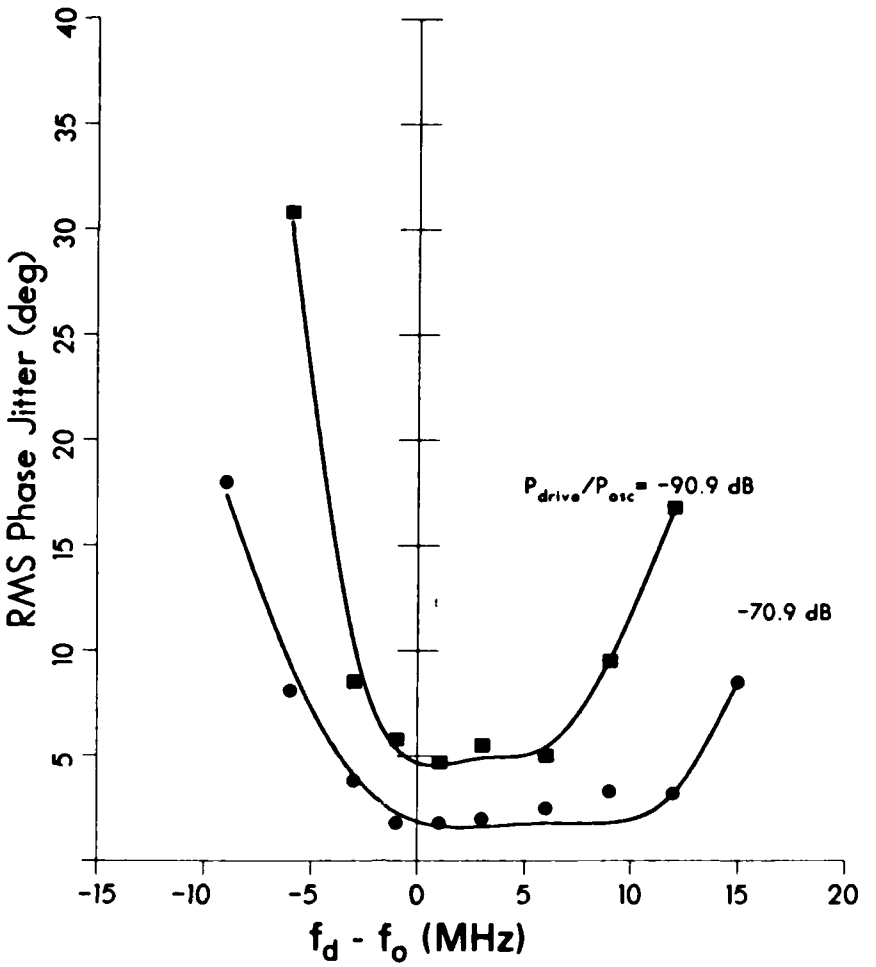

Fig. 12 — Priming cavity 3 by applying external signal to cavity 1

degree at a drive-to-oscillator power ratio of −70 dB. Figures 10, 11, and 12 each show a minimum in the phase jitter at a frequency slightly below the steady-state oscillator frequency. This feature has also been observed in magnetrons [35]. The explanation is that the phase control effect occurs during the oscillation buildup. The oscillation starts a short time after the beam voltage and current have reached their steady-state values. The voltage droops slightly during the time the oscillation is growing. We have found that the oscillation frequency increases as the voltage decreases. Thus the initial oscillation in the gyromonotron starts at a frequency slightly below the steady state oscillation frequency. The value we quote as the free oscillation frequency is actually the average frequency over the pulse, which is somewhat higher (~.1 to .2 MHz) than the frequency during the oscillation buildup. Thus, the highest degree of phase control is obtained when the drive frequency matches this buildup frequency. There is also a further asymmetry, apparent in the multicavity priming cases (Figs. 10 and 11), of overall better phase control at drive frequencies greater than the oscillation frequency. Possible explanations for this behavior are being investigated.

NOISE SUPPRESSION

Significant noise suppression is observed in the phase-locked gyromonotron. There is a decrease in the frequency, amplitude, and phase noise, as well as a decrease of jitter in the starting time of the pulsed oscillator. This type of improvement in noise characteristics has been noted in other phase-locked microwave systems [16,37]. It is found that priming, in addition to decreasing the variation in start-up phase of the oscillation, also decreases the fluctuation in oscillator starting time with respect to the beam voltage pulse. The noise measurements are made with the three-cavity circuit.

Two types of frequency noise are studied in the gyromonotron. One is a drift in frequency during the pulse caused by voltage droop on the MIG gun. The other is pulse-to-pulse variation in gyromonotron frequency caused by variation in electron beam parameters. The suppression of frequency noise of both types by injection of a locking signal is measured by using a frequency discriminator [40]. This technique consists of splitting the gyromonotron output into two branches, passing one branch through a phase shifter and nondispersive delay line, then recombining the two branches in a mixer. The phase shifter is used to null the oscilloscope display of the mixer output at a given frequency. Any frequency variation during gyromonotron operation translates into a phase shift at the mixer inputs and is displayed as a DC offset voltage on the oscilloscope. The pulse-to-pulse frequency jitter measurements are made by taking the standard deviation of a sequence of voltages from this diagnostic. Figure 13(a) shows the resulting decrease of frequency fluctuation caused by phase locking. Throughout the locking band the frequency jitter has been decreased by more than a factor of two from that of the free oscillation. The noise reduction is limited by noise intrinsic to the driving system. The large increase in frequency noise at the locking limits is a well-known phenomena [16]. The output of the frequency discriminator is shown in Fig. 14(a). There is a clear decrease of frequency drift during the pulse because of phase locking the gyromonotron.

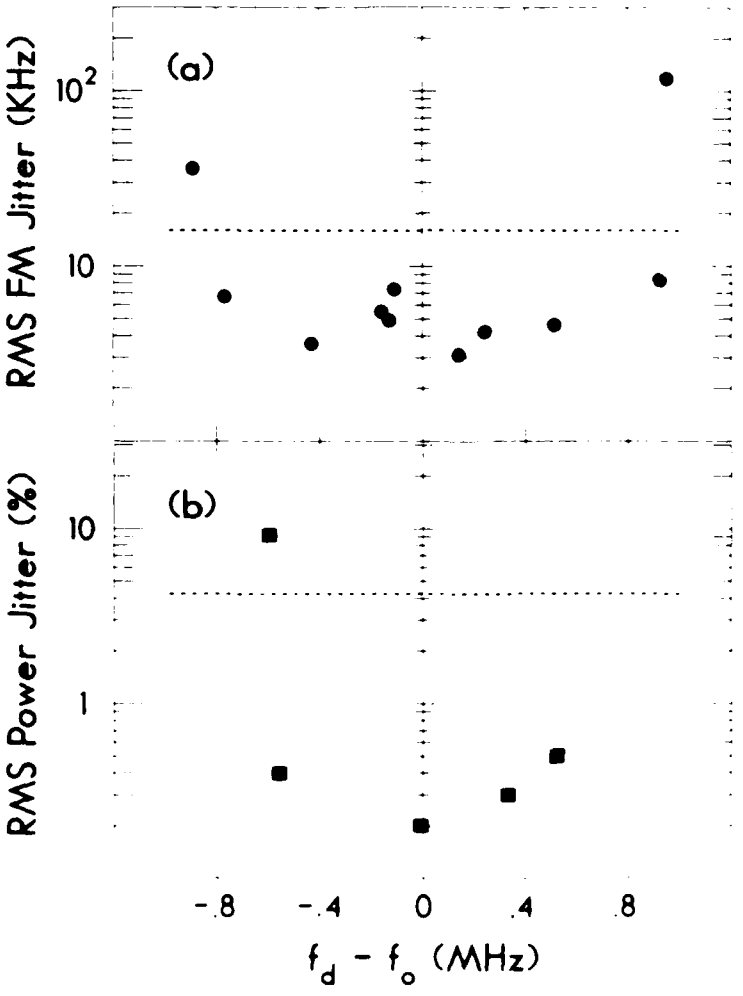

Fig. 13. Noise reduction, in the three-cavity configuration, through the phase locking band. (a) Frequency noise. (b) power level variations.

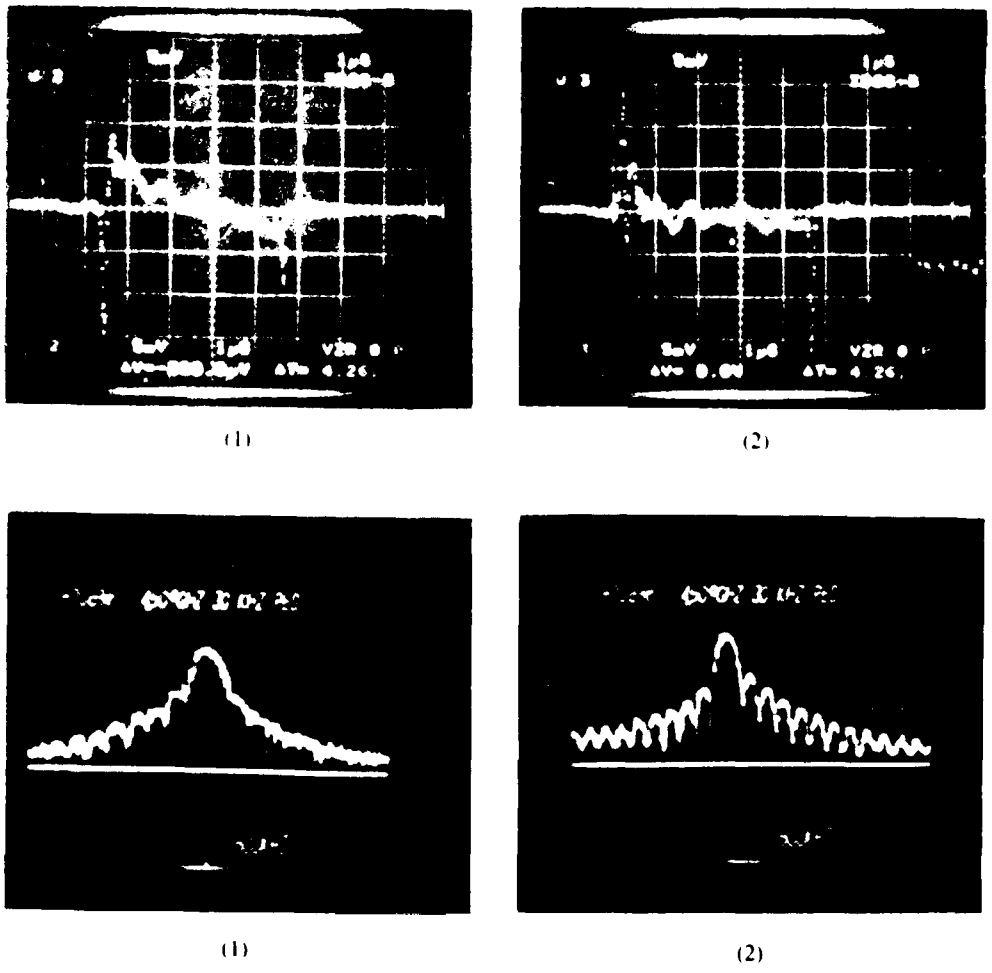

Fig. 14 — Frequency noise reduction due to phase locking (1) unlocked and (2) locked state. (a) Intrapulse frequency variation as measured with frequency discriminator (sensitivity 10 kHz div), (b) decrease in interline noise as measured with spectrum analyzer.

The decrease in frequency noise can also be seen in the sharpening of the gyromonotron spectrum. Figure 14(b) shows the increased definition of the spectral lines caused by the pulse repetition frequency when a locking signal is applied. There is a clear decrease of noise between the spectral lines (interline noise), indicating increased frequency stability.

Decrease of amplitude noise through the locking band is shown in Fig. 13(b). The noise is decreased from 4.3% jitter in power in the free oscillation to 0.3% in the center of the locking band. Once again the noise increased at the edges of the locking band. The measurement is made by taking the standard deviation of the voltage output from a crystal diode over ~100 pulses.

The pulse-to-pulse rms phase jitter is decreased to 1.5° in the phase-locked condition. This phase noise is measured by mixing the drive signal and gyromonotron output in phase quadrature and monitoring voltage fluctuations in the DC output from the mixer IF port [41-43]. This diagnostic simply transforms the phase variation between the driver and oscillator into a voltage variation that can be displayed on an oscilloscope. The phase stability in the phase-locked state approaches that of the gyroklystron amplifier [44].

The gyromonotron oscillation grows from a state of random noise; therefore, each pulse starts up at a slightly different time with respect to the rise of the voltage on the electron gun. This

starting-time noise translates into interline noise in the pulsed oscillator output spectrum [37]. The injection of an external signal, even far below the threshold required for locking, significantly decreases this start-up jitter. Figure 15 shows the stabilization in pulse starting time in response to small injected signals. This measurement is made by using a storage oscilloscope to display the voltage output of a crystal detector over a number of rf pulses. The width of this envelope is decreased by a factor of 10 even by signal-to-oscillator power ratios of < -50 dB.

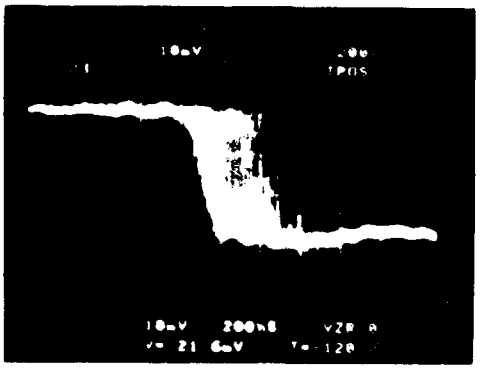

(a)

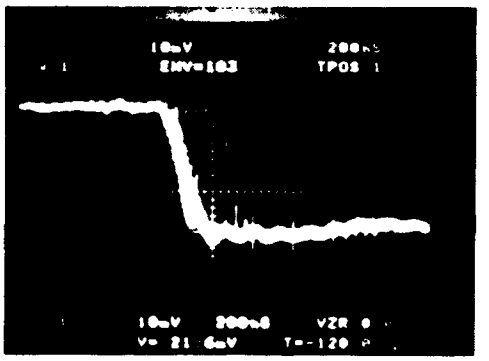

(b)

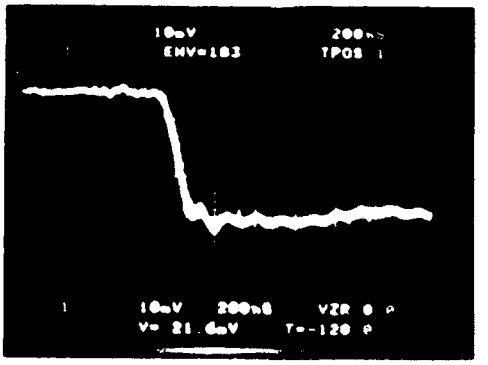

(c)

Fig. 15. Reduction of rf starting time jitter by applying a priming signal with $f_d = f_o$. (a) Free oscillation, jitter at front ~320 ns (enveloped over 100 waveforms); (b) $P_d/P_o = -72.7$ dB, jitter ~82 ns; (c) $P_d/P_o = -65.8$ dB, jitter ~40 ns.

REGIMES OF QUALITATIVELY DIFFERENT BEHAVIOR

The term "gyromonotron" has been used exclusively when referring to the single-cavity, self-excited oscillator. In discussing the more general behavior of the single-cavity, electron cyclotron maser, we use the term *gyrotron* modified by either *oscillator* or *amplifier* to signify the class of operation. Here, we make a short study of the different responses that the gyrotron may have to an externally applied signal. The three regimes investigated are those of *amplification*, *soft excitation*, and *hard excitation*, using the terminology from the theory of nonlinear oscillations [45]. These regimes can be identified in different areas of the oscillator plane defined by the uniform axial magnetic field and the beam current, all other parameters being fixed. The qualitatively different features of these regimes are discussed in this section.

Amplifier Regime

Amplifier behavior can be seen in a single-cavity gyrotron system when the beam current is below the start-oscillation threshold and cavity 1 beam parameters are such that the beam provides negative loading. A signal injected through the cavity output will experience gain upon reflection from the gyrotron amplifier. In a multiple-cavity system, the same criterion applies except the input cavity provides positive loading. Figure 16 shows the typical amplitude-frequency response of a gyrotron amplifier (three-cavity gyroklystron). The fact that the frequency corresponding to maximum gain is a function of drive power shows the effect of nonlinearity in the system. Features of the amplifier regime are

- the system has output only when the external signal is present,
- the output is related in phase to the drive signal, and
- the output increases linearly with small drive powers and proceeds smoothly to a saturation regime that can be due to overbunching of electrons (in the multicavity case) [46], phase trapping, or energy depletion [47].

Soft-Excitation Regime

The amplitude-frequency response of the soft excitation regime is shown in Fig. 17 (free oscillation in cavity 2, drive applied to cavity 1). The first characteristic is that the oscillation is self-excited and grows spontaneously from noise. For drive powers (applied to the gyrotron oscillator either by direct rf injection or premodulation of the electron beam) below a critical level (depending on the driver-oscillator frequency separation), the oscillation is autonomous. Above this critical power level, the gyrotron oscillation becomes phase locked; the oscillation frequency assumes that of the drive and becomes related in phase to the drive. There is some variation in the gyrotron output power level with drive power inside the locking band. In general, the gyrotron power could either increase or decrease inside the locking band, depending on how close to saturation (due to phase trapping or energy depletion) the gyrotron is operating.

A simple way to visualize the phenomena of soft excitation (in the absence of an external signal), is to use the phase space diagram shown in Fig. 18(a) [45]. The two coordinate axes are conjugate variables such as the electric field and its derivative that characterize the oscillation. The system starts at some point on the phase plane, specified by the initial conditions, then proceeds along the trajectory along which it lies. There are two equilibria, one at the origin and the other at the limit cycle represented by the dotted line. Only the latter equilibrium is stable, since trajectories wind toward the limit cycle from both directions (regions I and II). Thus the steady state is independent of initial conditions, and the oscillation is self-excited since the point (0,0) is unstable.

The problem of phase locking the oscillation is not easily seen in the phase plane since the external signal represents a nonautonomous term in the oscillator equation. The entire phase plane evolves in time with the external signal until a limit cycle corresponding to the locked steady state is formed.

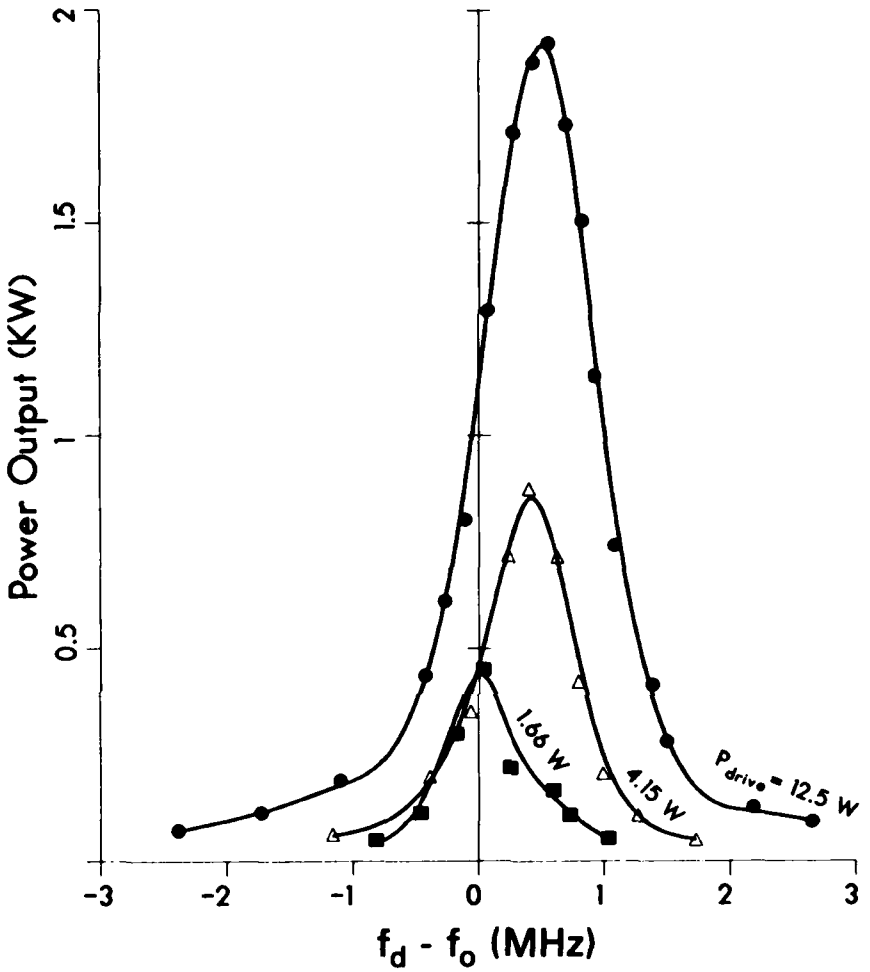

Fig. 16 — Amplifier amplitude-frequency response

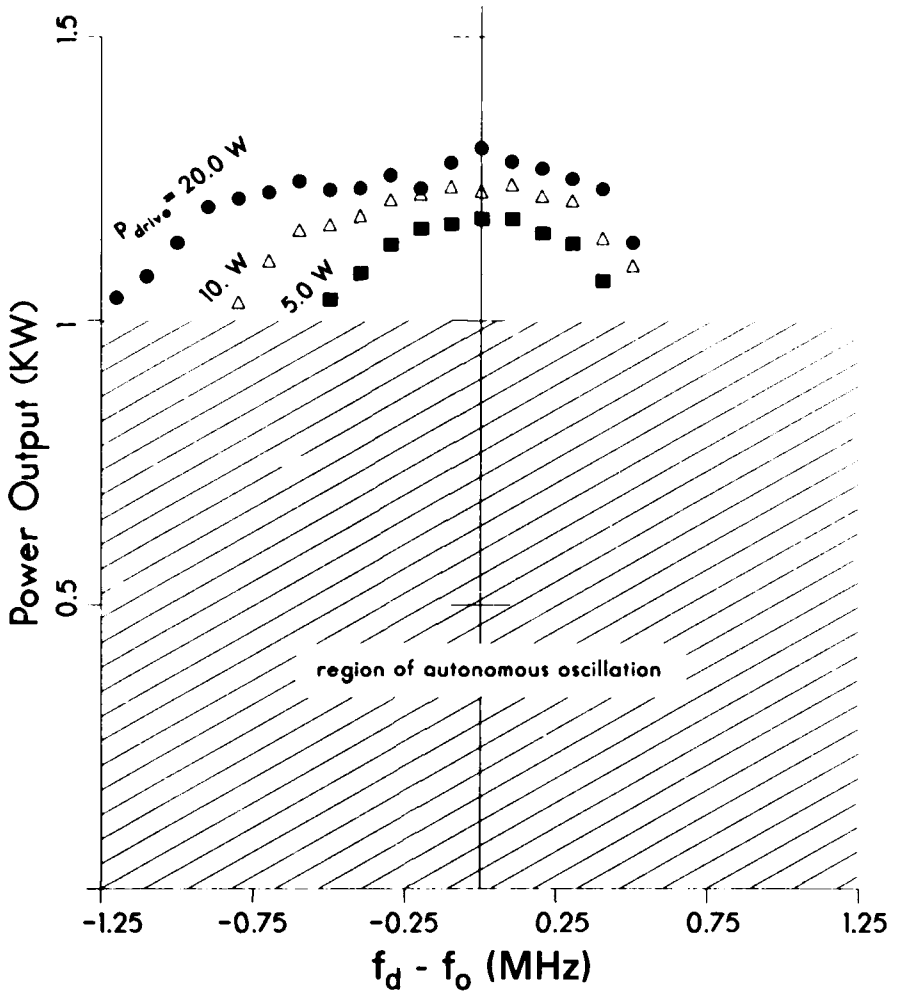

Fig. 17 — Amplitude-frequency response in soft excitation regime

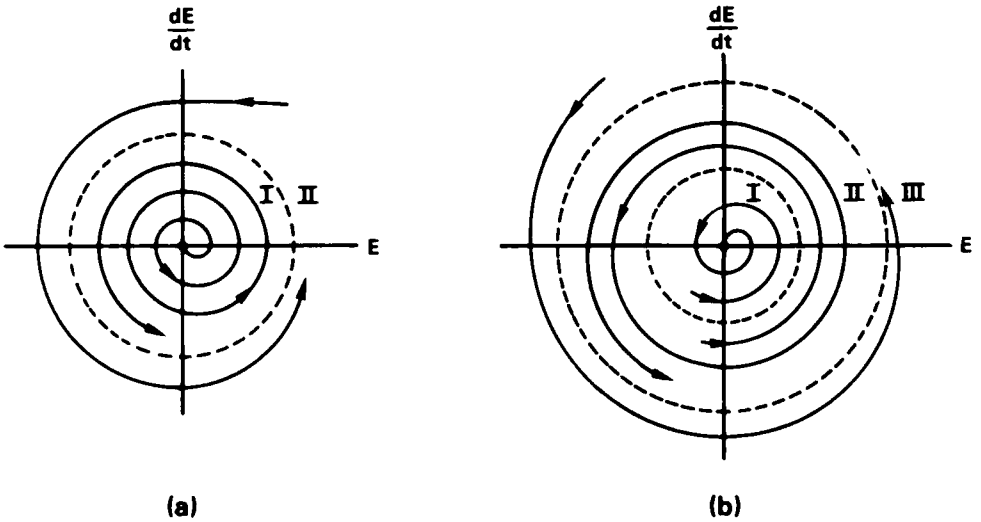

Fig. 18 — Phase space diagrams. (a) Soft excitation; (b) hard excitation

Soft excitation can be determined experimentally by the way the oscillator system responds to a slowly varied oscillator parameter [48] (which in the gyrotron oscillator could be the axial magnetic field, beam current, output load, etc.). If the nature of the oscillator is such that the amplitude changes continuously from zero as the parameter is varied, the oscillation is a case of soft excitation. This behavior is seen in the gyrotron as the beam current, for example, is increased through the start-oscillation current. Note that this test of soft excitation can be done in the steady state and does not examine the time-dependent features shown in the phase plane example.

Hard-Excitation Regime

Hard excitation is the situation where the origin is a stable equilibrium (as shown in Fig. 18(b)). There are two limit cycles, one unstable and the other stable. If the initial condition of the oscillator is something other than $(E = 0, dE/dt = 0)$, the system may move to a new equilibrium if the initial conditions are either in regions II or III. The new equilibrium is now a steady-state oscillation, shown by the outermost limit cycle. An amplitude threshold exists that the initial condition must exceed (large enough to reach region II) for the system of Fig. 18(b) to begin to oscillate. The final steady state, however, is insensitive to any other characteristics of the initial condition. The hard excitation regime can be identified when a normally stable system is driven into a state of free oscillation by an external perturbation of arbitrary characteristics other than that it exceeds a given amplitude. An external signal, present during the course of the oscillation, can phase lock the oscillation in the hard excitation regime just as in the soft.

Hard excitation also can be identified by slowly varying an otherwise static oscillator parameter. The oscillation amplitude is observed to change discontinuously from a steady-state value [48].

Figure 19 shows the experimentally observed phenomenon of hard excitation in the gyrotron oscillator. The oscillation is in cavity 3, and the drive is applied to cavity 1. The drive signal is present only during the first 1 μs of the high-voltage pulse across the electron gun (Fig. 19(c) shows the synchronization). Thus the drive signal provides an initial condition for the oscillator other than $(E = 0, dE/dt = 0)$. No oscillation is present in the absence of the drive signal. For a drive signal >22 mW (see Fig. 19(b)), the oscillation is excited for the duration of the electron beam pulse. Unlike the bulk of the pulse, the pulse front edge is affected by the amplitude of the drive signal. No further change takes place in the oscillation as the drive amplitude is increased further or frequency is varied (within the cavity 1 bandwidth).

A drive curve of the three-cavity device operating in the hard excitation regime is shown in Fig. 20. There is weak amplification of the drive signal for small drive powers (the drive signal is applied over the entire electron beam pulse in this case). When a critical drive power is reached, the oscillation initiates and the output power increases dramatically. The phase discriminator reveals that the output of the device is phase locked to the drive throughout the drive curve. Thus, the drive power which initiates the oscillation is enough to cause it to phase lock. There is no reason to assume that this is generally the case. If the drive frequency were varied significantly from that of the oscillation, for example, there might still be initiation of the oscillation but no phase locking.

Figure 21 shows an example of the amplitude-frequency response in the hard excitation regime. These data are again from a cavity 3 oscillation initiated by a drive signal applied to cavity 1. Note that the oscillation is excited by a wide range of drive frequencies. The oscillation frequency, however, is never affected by the drive signal except in the narrow region about $f_d - f_0 = 0$ where the gyrotron becomes phase locked. In this experiment, the drive signal is on throughout the oscillation pulse so that there is some dependence of the oscillator power of the drive power. If the gyrotron oscillator cavity is long enough to produce a beam-wave saturation condition, this power dependence probably will not be evident. If an amplifier is designed to operate in the hard excitation regime, bandwidths cannot be expected beyond that over which the oscillation is phase locked. Figure 21 shows that this is a small fraction of the cavity bandwidth.

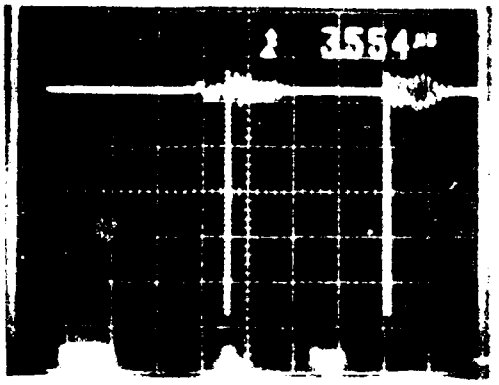

(a)

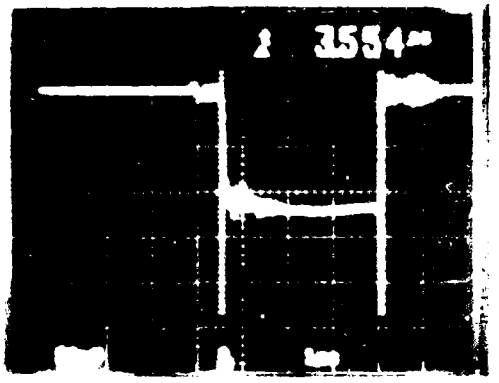

(b)

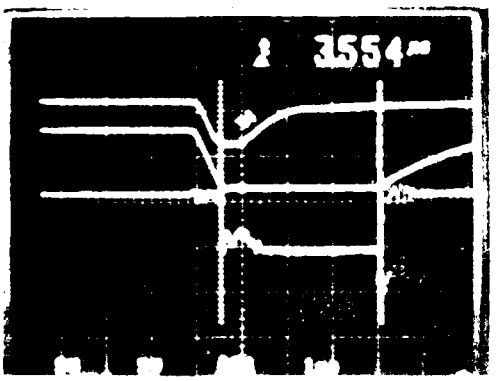

(c)

Fig. 19 — Oscillographs of diode traces monitoring gyrotron output showing hard excitation. (a) $P_d < 22$ mW, $f_d = 4.47$ GHz; (b) $P_d = 236$ mW, excitation of 12.1 kW oscillation with $f_0 = f_d$; (c) synchronization of (from top) drive rf, electron gun high voltage, output rf

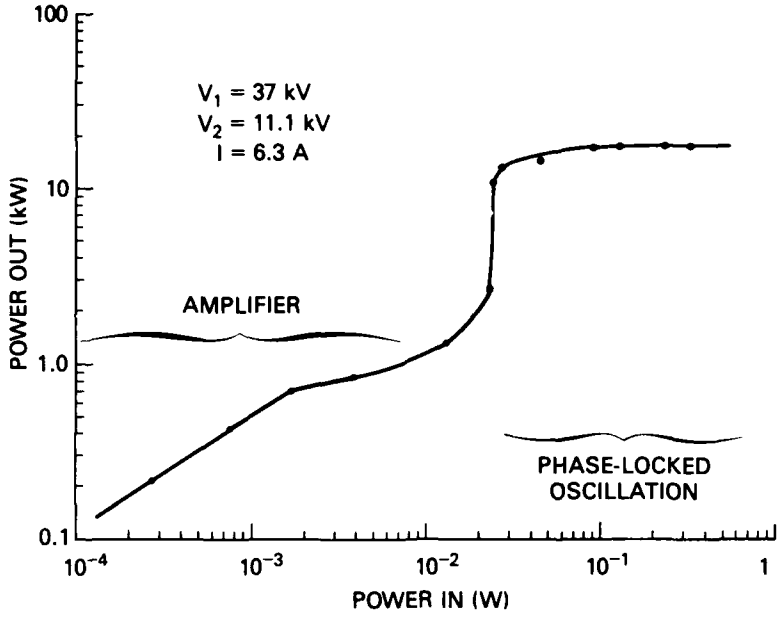

Fig. 20 — Drive curve in hard excitation regime for same parameters as Fig. 19 except with CW drive

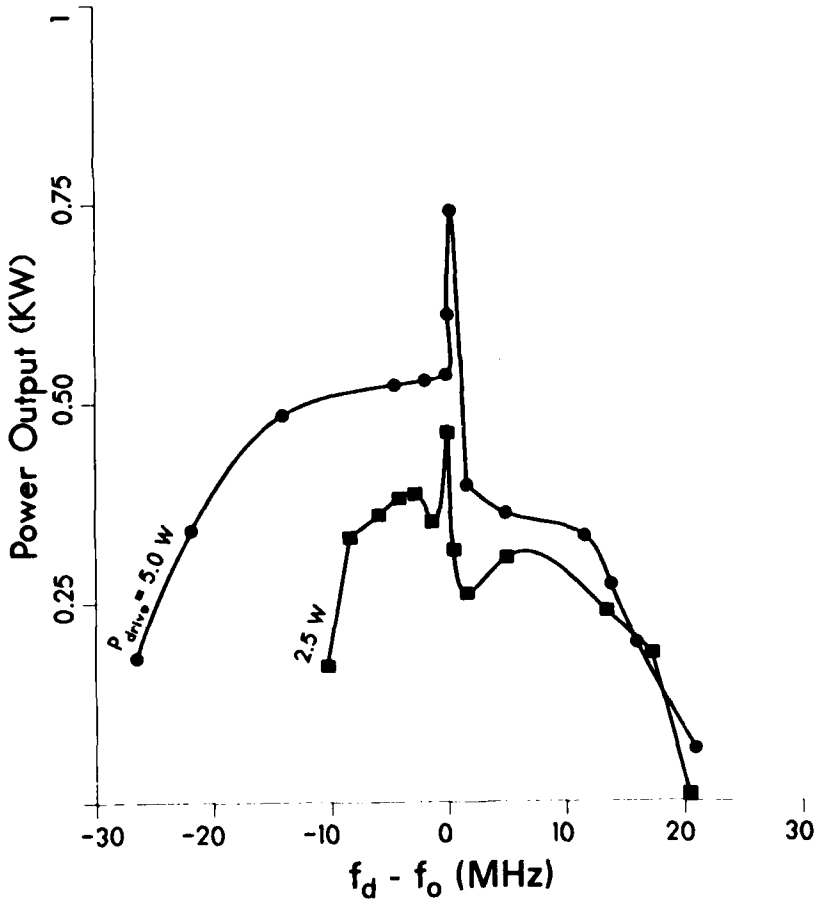

Fig. 21 — Amplitude-frequency response in hard excitation regime

The Gyrotron Oscillator Plane

The three regimes of qualitatively different behavior discussed above are shown on the gyrotron oscillator plane of Figs. 22 and 23. These data are taken for a cavity 1 oscillation directly injecting an rf signal. A premodulation experiment cannot be done (using our cavities) in this case, because of the stability problems inherent in the pre-bunching cavities as the magnetic field and beam current are varied. Two current limits are identified in the experiment that delineate the different regions. The highest beam current possible while operating in the amplifier regime is termed I_{min}. The measured start-oscillation current of the gyrotron oscillator in the absence of the external signal is I_{start}. The regimes shown are similar in location to those predicted [49]. Iso-efficiency contours are shown in Figs. 22 and 23. With our short cavity length (too short to produce beam-wave saturation), we cannot determine whether the high-efficiency region moves as predicted [49] to lower beam current in the presence of an external signal.

Figure 23 shows the operating frequency of the gyrotron in both the oscillator and the amplifier modes when driven at a constant power and at the frequency of maximum oscillator efficiency. The efficiency maximizes when the drive frequency equals the oscillation frequency; this will not necessarily be the case for larger drive power. An interesting feature of this figure is that the curves of constant frequency are continuous through the different regimes.

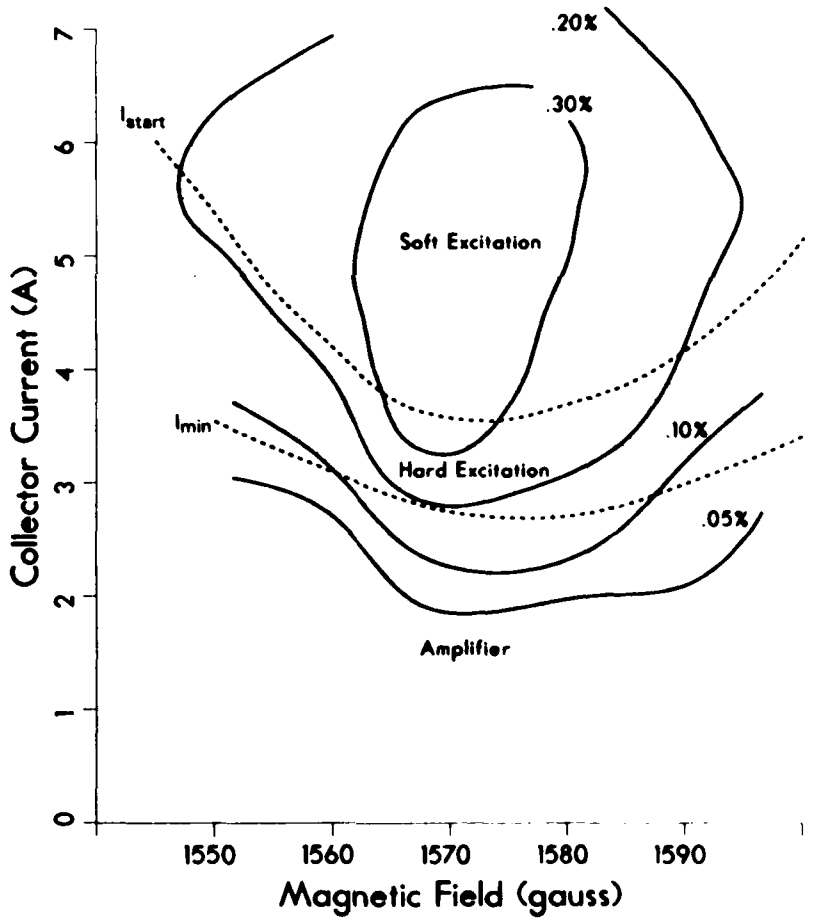

Fig. 22 — Gyrotron oscillator plane when driven by external rf with drive frequency adjusted for maximum oscillator efficiency, P_d = 12.5 W, $V_{cathode}$ = 29.2 kV, $V_{mode-anode}$ = 20.5 kV showing iso-efficiency contours

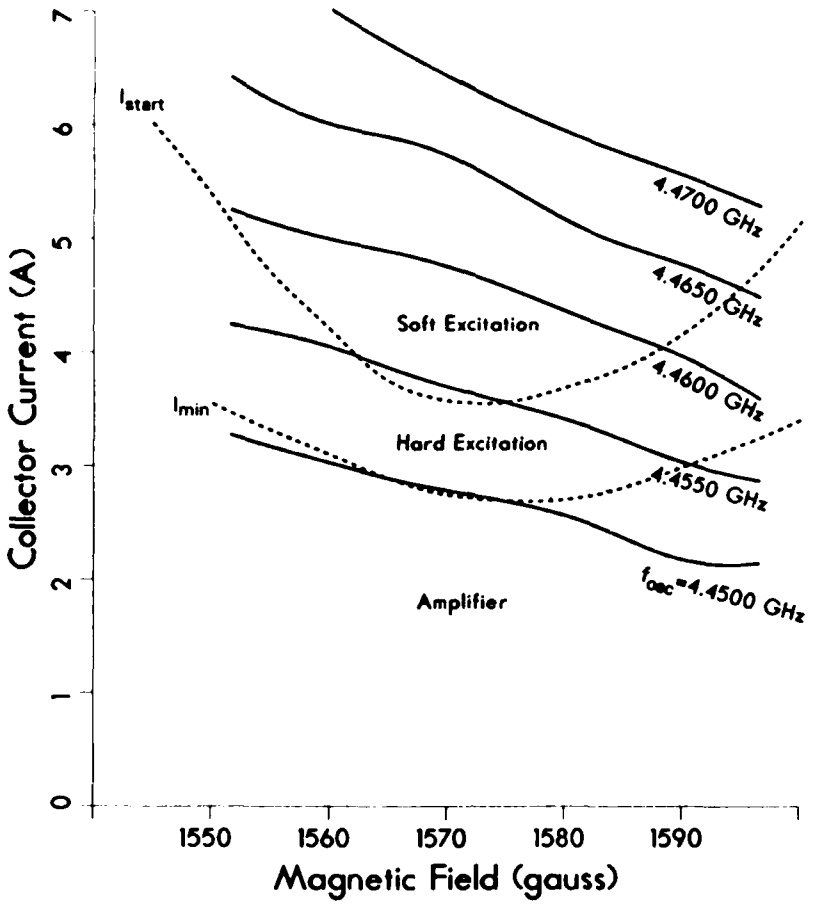

Fig. 23 — Gyrotron oscillator plane when driven by external rf with drive frequency adjusted for maximum oscillator efficiency, P_d = 12.5 W, $V_{cathode}$ = 29.2 kV, $V_{mode-anode}$ = 20.5 kV showing contours of constant frequency

CONCLUSIONS

The response of a gyrotron to the application of an external signal, applied both by direct injection of rf into the gyrotron and by premodulation of the electron beam, has been studied. It is found that phase control can be achieved over the gyromonotron by means of phase locking and priming. Both of these methods of phase control are improved by introducing an external signal into a prebunching cavity rather than directly into the gyromonotron. This premodulation technique allows phase locking at input power levels 15 dB below that predicted by Adler's theory for a single cavity. Also, oscillator priming to limit rms phase jitter to 2° can be accomplished at input powers ~50 dB below that required in magnetrons. Oscillator noise is significantly reduced by both control methods. Finally, the different regimes of gyrotron behavior are examined experimentally and located in the gyrotron oscillator plane.

Further work will include controlling a particular oscillator mode in an overmoded gyrotron and enhancing the efficiency by premodulating the electron beam.

ACKNOWLEDGMENTS

The authors thank V.L. Granatstein for careful reading of the manuscript and A.K. Ganguly, R.K. Parker, and S.Y. Park for helpful discussions. The work of S. Swiadek and F. Wood on construction of the experiment is also acknowledged. This work was supported by the Office of Naval Research and the Office of Naval Technology.

REFERENCES

1. A.V. Gaponov, Report presented at the All-Union Session of Popov's Society, Moscow, 1959.
2. J.L. Hirshfield and J.M. Wachtel, *Phys. Rev. Lett.* **12**, 533 (1964).
3. R.H. Pantell, *Proc. IRE* **47**, 1146 (1959).
4. A.V. Gaponov, M.I. Petelin, and V.K. Yulpatov, *Radiophys. Quant. Electron.* **10**, 794 (1967).
5. K.E. Kreischer et al., *Int. J. Electron.* **57**, 835 (1984).
6. A.G. Luchinin, O.V. Malygin, G.S. Nusinovich, and V.A. Flyagin, *Sov. Phys. Tech. Phys.* **28**, 1001 (1983).
7. K. Felch et al., in *Conference Digest of the Eleventh International Conference on Infrared and Millimeter Waves*, Pisa, Italy, 1986, to be published.
8. A.K. Ganguly and K.R. Chu, *Int. J. Electron.* **51**, 503 (1981).
9. V.S. Ergakov and M.A. Moiseev, *Izv. Vyssh. Uchebn. Zaved. Radiofiz.* **18**, 120-131 (1975); (translated in *Radiophysics and Quantum Electronics* **18**, 89-97 (1975)).
10. A.V. Gaponov et al., *Int. J. Electron.* **51**, 277 (1981).
11. Y. Carmel et al., *Phys. Rev. Lett.* **50**, 112 (1983).
12. E.M. Demidovich, C.S. Kovalev, A.A. Kuryev, and F.G. Shevchenko, *Radio Eng. Electron. Phys.* **18**, 1542 (1973).
13. R.S. Symons and H.R. Jory, in *Advances in Electronic and Electron Physics*, L. Marton and C. Marton, eds. (Academic Press, New York, 1981), vol. 55, p. 1.
14. V.S. Bazhanov, V.S. Ergakov, and M.A. Moiseev, *Radiophys. Quant. Electron.* **20**, 90 (1977).
15. J.C. Slater, Mass. Inst. Technol., Research Lab. Electronics, Tech. Rept. No. 35 (1947).
16. K. Kurokawa, *Proc. IEEE* **61**, 1386 (1973).
17. W.M. Bollen et al., *IEEE Trans. Plasma Sci.* **PS-13**, 417 (1985).
18. A.K. Ganguly, A.W. Filflet, and A.H. McCurdy, *IEEE Trans. Plasma Sci.* **PS-13**, 409 (1985).
19. B. van der Pol, *Philos. Mag.* **III**, 65 (1927).
20. E.V. Appleton, *Proc. Camb. Phil. Soc.* **21**, 231 (1923).

21. R. Adler, *Proc. IRE* **34**, 351 (1946).

22. H.L. Stover and W.H. Steier, *Appl. Phys. Lett.* **8**, 91 (1966).

23. M. Sargent III, M.O. Scully, and W.E. Lamb, Jr., *Laser Physics* (Addison-Wesley, Reading, MA, 1974), p. 120-141.

24. J.C. Slater, *Microwave Electronics* (Van Nostrand, New York, 1950), p. 205.

25. Anaren Microwave Components, Cat. No. 17, 197 (1984).

26. M.E. Read, R. Seeley, and W.M. Manheimer, *IEEE Trans. Plasma Sci.* **PS-13**, 398, (1985).

27. K.E. Kreischer, R.J. Temkin, H.R. Fetterman, and W.J. Mulligan, *IEEE Trans. Microwave Theory Tech.* **MTT-32**, 481 (1984).

28. I.G. Zarnitsyna and G.S. Nusinovich, *Radiophys. Quant. Electron.* **17**, 1418 (1974).

29. G.S. Nusinovich, *Radiophys. Quant. Electron.* **19**, 1301 (1976).

30. E.E. David Jr., *Proc. IRE* **40**, 669 (1952).

31. J.E. Evans, R.C. Fletcher, and F.F. Rieke, Mass. Inst. Technol., Rad. Lab. Rept. No. 1051 (1946).

32. H. Pollmann and B.G. Bosch, *IEEE Trans. Electron Dev.* **ED-14**, 609 (1967).

33. D.M. Brookbanks, in *Proc. Conf. Military Microwaves 82*, London, England (1982), p. 230.

34. D. Anderson, M. Lisak, and T. Lewin, *IEEE Trans. Microwave Theory Tech.* **MTT-31**, 963 (1983).

35. J.C. Slater, *Micronotes* **4**, Microwave Associates, Burlington, MA (1966).

36. B. Vyse, V.H. Smith, and M.O. White, in *Proc. Conf. Military Microwaves 82*, London, England (1982), p. 217.

37. B. Vyse and H. Levinson, *IEEE Trans. Microwave Theory Tech.* **MTT-29**, 739 (1981).

38. D.M. Guillory and R.W. McMillan, in *Conference Digest of the Tenth International Conference on Infrared and Millimeter Waves*, Lake Buena Vista, Florida (1985), p. 48.

39. J.K. Parker, Varian Associates, Beverly, Massachusetts, private communication, 1985.

40. Anaren Microwave Components, Cat. No. 17, 154 (1984).

41. D.A. Howe, NBS Tech. Note 679, March 1976.

42. J.H. Shoaf, D. Halford, and A.S. Risley, NBS Tech. Note 632, Jan. 1973.

43. G.E. Thomas, private communication.

44. J. McAdoo et al., *IEEE Trans. Nucl. Sci.* **NS-32**, 2963 (1985).

45. N. Minorsky, *Nonlinear Oscillations* (Van Nostrand, Princeton, NJ, 1962), p. 71.

46. D.S. Furuno. D.B. McDermott, N.C. Luhmann, Jr., and P. Vitello, *Int. J Electron.* **57**, 1151 (1984).

47. P. Sprangle and A.T. Drobot, *IEEE Trans. Microwave Theory Tech.* **MTT-25**, 528 (1977).

48. N.N. Bogolyubov and Y.A. Mitropolski, *Asymptotic Methods in the Theory of Nonlinear Oscillations* (Hindustan, Delhi, 1961), pp. 91-102.

49. V.S. Yergakov, M.A. Moiseyev, and V.I. Khizhnyak, *Radio Eng. Electron. Phys.* **23**, 92 (1978).

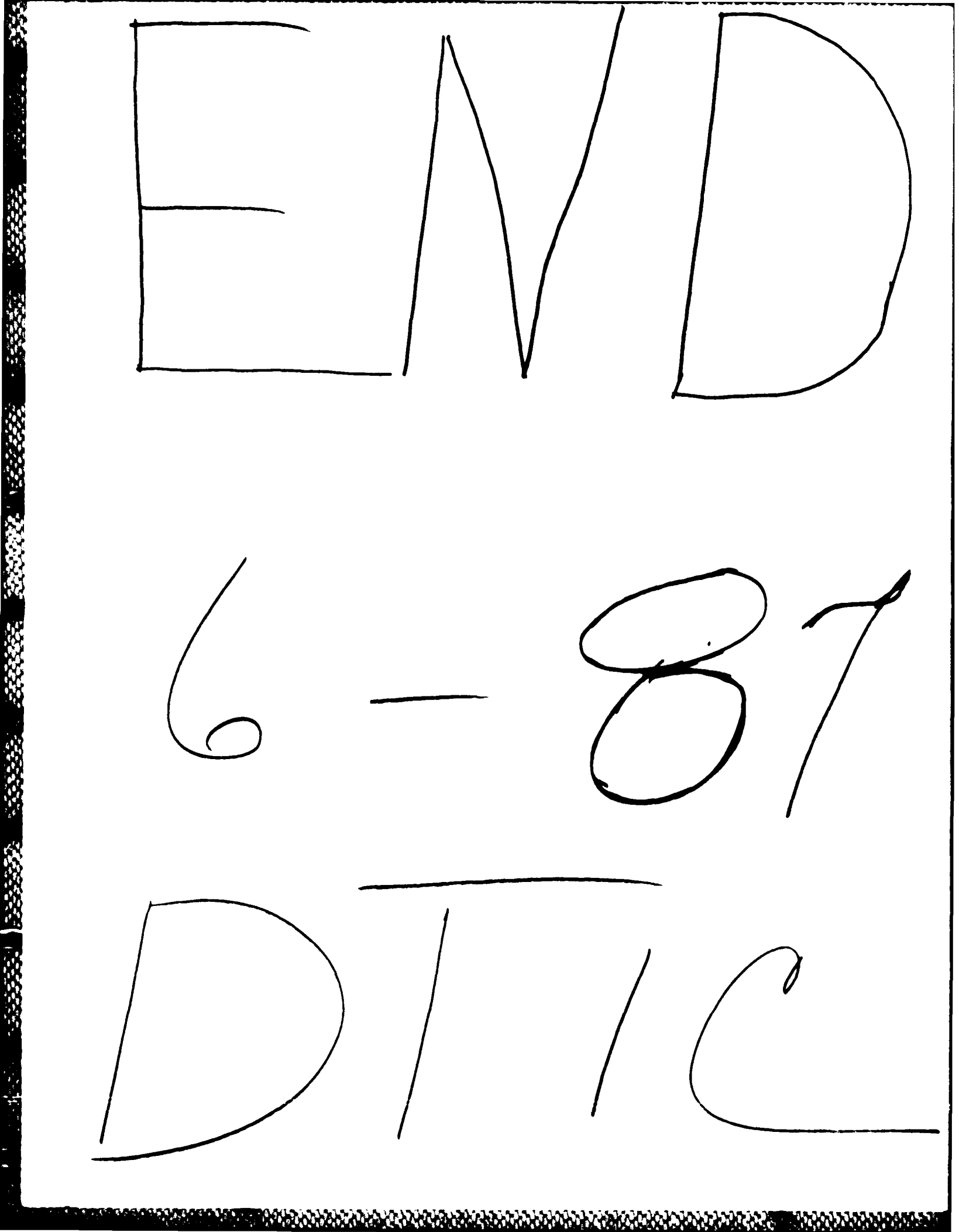
END
6-87
DTIC